7-1-1977

Low-Frequency Response Functions of Random Magnetic Systems

A. Brooks Harris
University of Pennsylvania, harris@sas.upenn.edu

Scott R. Kirkpatrick

Recommended Citation
Harris, A., & Kirkpatrick, S. R. (1977). Low-Frequency Response Functions of Random Magnetic Systems. *Physical Review B, 16* (1), 542-576. http://dx.doi.org/10.1103/PhysRevB.16.542

Low-Frequency Response Functions of Random Magnetic Systems

Abstract
The frequencies of long-wavelength spin waves in random magnets are studied through their relation to the static magnetic elastic constants A, the domain-wall stiffness, and (for antiferromagnets) $\chi_\perp$, the perpendicular susceptibility. We treat the classical limit of large spin and low temperature. In the case of random dilution A and $\chi_\perp$ are evaluated numerically as a function of magnetic concentration p for common lattices. Exact analytic results for the static susceptibility, $\chi(q)$, where q is the wave vector, are given for some models of disorder in one dimension and, for higher dimensionality, in the limit of low concentrations of vacancies. One general conclusion is that local fluctuations in the spin magnitude significantly affect $\chi_\perp$, causing it to diverge for isotropic random systems in two or fewer dimensions. If critical exponents are defined for $p \to p_c$ by $A \sim |p-p_c|^\sigma$, $\chi_\perp \sim |p-p_c|^{-\tau}$, $P \sim |p-p_c|^\beta$, and $\xi \sim |p-p_c|^{-\nu}$, where p_c is the percolation threshold, P is the percolation probability, and ξ is the correlation length, then our numerical results in three dimensions yield $\sigma = 1.6 \pm 0.1$ and $\tau = 0.5 \pm 0.2$. A simple physical argument shows that $\tau \geq \sigma - \beta + (2-d)\nu$. Our data are consistent with the possibility that this is an equality. Using mean-field-theory values for the exponents in this relation leads to a critical dimensionality $d_c = 6$. We study p_c, A, and $\chi_\perp$ in diluted YIG and mixed garnets and give a detailed discussion of the regime near angular momentum compensation, where a low-frequency optical mode with both $\omega \propto q$ and $\omega \propto q^2$ regimes occurs. Our work contradicts the common assumption of a concentration-independent relationship between T_c and A or D, the spin-wave stiffness. We also present nonlinear calculations which allow us to study the dependence of $\chi_\perp$ on magnetic field. Our calculations agree with the experimental results on diluted $KMnF_3$ and K_2MnF_4 and show that the observed nonlinearity is largely the result of local ferrimagnetic fluctuations. A novel configuration for elastic neutron scattering in the presence of a transverse magnetic field is proposed to permit direct observation of the magnitude and characteristic length scale of these fluctuations.

Disciplines
Physics

Low-frequency response functions of random magnetic systems

A. Brooks Harris*
Department of Physics, University of Pennsylvania, Philadelphia, Pennsylvania 19174

Scott Kirkpatrick
IBM Thomas J. Watson Research Center, Yorktown Heights, New York 10598

(Received 1 March 1976)

The frequencies of long-wavelength spin waves in random magnets are studied through their relation to the static magnetic elastic constants A, the domain-wall stiffness, and (for antiferromagnets) $\chi_\perp$, the perpendicular susceptibility. We treat the classical limit of large spin and low temperature. In the case of random dilution A and $\chi_\perp$ are evaluated numerically as a function of magnetic concentration p for common lattices. Exact analytic results for the static susceptibility, $\chi(q)$, where q is the wave vector, are given for some models of disorder in one dimension and, for higher dimensionality, in the limit of low concentrations of vacancies. One general conclusion is that local fluctuations in the spin magnitude significantly affect $\chi_\perp$, causing it to diverge for isotropic random systems in two or fewer dimensions. If critical exponents are defined for $p \to p_c$ by $A \sim |p - p_c|^\sigma$, $\chi_\perp \sim |p - p_c|^{-\tau}$, $P \sim |p - p_c|^\beta$, and $\xi \sim |p - p_c|^{-\nu}$, where p_c is the percolation threshold, P is the percolation probability, and ξ is the correlation length, then our numerical results in three dimensions yield $\sigma = 1.6 \pm 0.1$ and $\tau = 0.5 \pm 0.2$. A simple physical argument shows that $\tau \geq \sigma - \beta + (2 - d)\nu$. Our data are consistent with the possibility that this is an equality. Using mean-field-theory values for the exponents in this relation leads to a critical dimensionality $d_c = 6$. We study p_c, A, and $\chi_\perp$ in diluted YIG and mixed garnets and give a detailed discussion of the regime near angular momentum compensation, where a low-frequency optical mode with both $\omega \propto q$ and $\omega \propto q^2$ regimes occurs. Our work contradicts the common assumption of a concentration-independent relationship between T_c and A or D, the spin-wave stiffness. We also present nonlinear calculations which allow us to study the dependence of $\chi_\perp$ on magnetic field. Our calculations agree with the experimental results on diluted $KMnF_3$ and K_2MnF_4 and show that the observed nonlinearity is largely the result of local ferrimagnetic fluctuations. A novel configuration for elastic neutron scattering in the presence of a transverse magnetic field is proposed to permit direct observation of the magnitude and characteristic length scale of these fluctuations.

I. INTRODUCTION

This study has been motivated by recent accurate experimental measurements of the static and dynamic properties of magnetic alloys in which the microscopic interactions between spins are well known from previous studies of the pure substances. Examples of such work are the measurements of the susceptibility and Néel temperature by Breed and co-workers[1-3] on $KMnF_3$, a three-dimensional (3D) antiferromagnet (AF), and on K_2MnF_4, a 2D AF, when a fraction $1-p$ of Mn ions are replaced by nonmagnetic ions such as Zn or Mg. Similar experiments have been done for diluted and mixed garnets.[4] Dynamical measurements of the spin-wave spectrum have been carried out for alloys based on[5] MnF_2 and on Rb_2MnF_4.[6,7]

Many more experiments have been done on mixed systems than on pure elements, and even amorphous magnets are now being studied,[8] yet essentially all measurements have been interpreted in terms of virtual crystal pictures, or by the introduction of effective exchange parameters. In this paper we set up an exact formalism in which effects of disorder can be treated by numerical calculation of certain physical quantities. We shall work out several simple cases in detail. Some of the results given here have been summarized previously.[9,10]

We first give a general framework for discussing low-energy excitations in terms of static magnetic response functions. Some of this material can be found in various places in the literature. We collect it here for consistency in notation, and for use in the later sections. Microscopic expressions for the evaluation of these response functions for classical spin systems at zero temperature are then derived in the context of a specific model of disorder. Some exact analytic results for disordered one-dimensional systems are presented.

The case of dilution of the magnetic atoms with nonmagnetic species is treated in some detail, since experiments on both antiferromagnets and ferrimagnets of this type have been performed. Exact results in the limit of low concentrations of nonmagnetic ions are given. More generally, we use computer simulation to calculate the static response functions for these systems at arbitrary concentrations. Results for the exchange stiffness A and the antiferromagnetic perpendicular susceptibility $\chi_\perp$ are examined for several models.

Ferromagnets have been treated previously,[11,12]

but the results for ferri- and antiferromagnets are new. There are some surprising features. In contradiction to the prediction of effective-medium theory, $\chi_\perp$ increases with increasing vacancy concentration, and diverges at the percolation threshold. Experimentally, $\chi_\perp$ is found to be strongly magnetic field dependent at moderate dilutions. We analyze this effect by a numerical treatment of the nonlinear response. We find that the interaction between vacancies in two-dimensional antiferromagnets is sufficiently long ranged that the usual hydrodynamic modes[13] at long wavelength are modified by any finite concentration of missing magnetic atoms. This anomaly does not occur in the presence of crystalline anisotropy. A careful calculation of the response functions in the presence of anisotropy is presented. We also give predictions of the energy of a low-frequency optical mode, which should be experimentally observable in the mixed Yb-Gd garnets.

We have also studied the behavior of the static magnetic response functions near the percolation threshold.[14] We obtain numerical estimates of the exponents describing the asymptotic behavior of A and $\chi_\perp$. Using physical arguments based on the existence of a correlation length, we obtain an inequality involving the exponents for $\chi_\perp$, A, and the geometrical properties of percolation networks. Our numerical data are compatible with the assumption that this inequality is in fact an equality.

Briefly, this paper is organized as follows. In Sec. II we define the model used to describe disordered systems. In Sec. III we use continuum theory to relate the spin-wave frequencies at long wavelength to static magnetic response functions, microscopic expressions for which are derived in Sec. IV. Some exact evaluations of the magnetic response functions are given in Sec. V, primarily for one-dimensional disordered magnets, and in Sec. VI for magnets in the limit of low vacancy concentration. Numerical results for common two- and three-dimensional lattices are given in Sec. VII for concentrations away from the percolation limit, and in Sec. VIII close to the percolation threshold. Applications of our techniques to more realistic systems are described in Secs. IX and X. In Sec. IX we study numerically the nonlinear response of a dilute antiferromagnet to an external magnetic field. These calculations are then compared with experimental data in which the field dependence of $\chi_\perp$ is a prominent effect. In Sec. X we calculate A for various types of dilution in YIG. We study the behavior of the low-frequency optical mode which occurs in mixed garnets whose composition is near that of spin compensation. Our conclusions are summarized in Sec. XI.

A microscopic derivation of the spin-wave frequencies for antiferromagnets at long wavelengths, in which the results of continuum theory are recovered, is given in Appendix A. In Appendix B an exact calculation of the response of a linear chain to an external transverse field of arbitrary wave vector is presented. In other appendices we discuss $\chi_\perp$. In Appendix C, we give an evaluation of $\chi_\perp$ for a random 2D system which shows that it diverges logarithmically in the presence of static spatial fluctuations in the magnitude of spin density (as occurs with dilution). We argue (in Appendix D) that it increases monotonically with vacancy concentration, at least on the average.

II. DEFINITION OF THE MODEL

The microscopic Hamiltonian we consider is the following:

$$H = -\sum_{i,j} J_{ij}\vec{S}_i\cdot\vec{S}_j - \sum_i \Delta_i S_i^z \sigma_i , \tag{1}$$

where, in the most general case, both the exchange integrals J_{ij} and the microscopic anisotropy energy Δ_i, as well as the spin magnitudes, are random variables, and $\sigma_i = +1$ for spins whose equilibrium orientation is in the positive z direction, and $\sigma_i = -1$ for oppositely directed spins.

In the special case of nonmagnetic dilution we may write the Hamiltonian in the form

$$H = -\sum_{i,j} J_{ij} p_i p_j \vec{S}_i\cdot\vec{S}_j - \sum_i \Delta_i p_i \sigma_i S_i^z , \tag{2}$$

where each p_i is a random variable assuming the values 1 or 0 when the site is or is not occupied by a magnetic ion. The techniques and relations developed in this paper are valid for all random systems of the form (1), but for simplicity we shall frequently specialize the discussion to the case of random dilution.

III. CONTINUUM THEORY

In this section we derive relations between the frequencies of low-energy long-wavelength spin waves, and static properties of the system: its magnetization M, exchange stiffness A, susceptibility χ, and anisotropy energy K. The latter quantities prove easier to calculate by numerical methods than the former, and are themselves experimentally accessible. Three cases, ferromagnets, antiferromagnets, and ferrimagnets, are treated.

In the absence of anisotropy, our derivation is a naive zero-temperature version of the finite-temperature hydrodynamic treatment of Halperin and Hohenberg,[13] i.e., a consistent expansion to lowest nonvanishing order in frequency ω and wave vector q. In the presence of anisotropy, all spin

waves have finite frequency, so such an expansion is not possible. In the latter case, the error in our derivation remains small as long as K is small with respect to typical exchange energies, but it is difficult to estimate in general. We shall discuss this point further in Sec. VI, where exact results from single-defect theory are presented.

Low-frequency long-wavelength excitations can be derived from the classical expressions for the magnetostatic energy. Consider a ferromagnet with magnetization $\vec{M}(\vec{r}) = M\hat{n}(\vec{r})$, where M is constant over macroscopic distances and $\hat{n}$ is a unit vector parallel to the spin direction at $\vec{r}$. If the direction of $\hat{n}$ is slowly varying, the exchange energy may be expressed, in the continuum approximation, as

$$E_{ex} = E_0 + A \sum_{\alpha} \int |\vec{\nabla} \hat{n}_{\alpha}(\vec{r})|^2 d\vec{r}\,, \tag{3}$$

where E_0 is the energy of the fully aligned system, henceforth taken to be zero, $\alpha = x$, y, or z labels the Cartesian coordinates, and A is the exchange stiffness constant.[15] The simplest type of anisotropy energy for uniaxial symmetry is expressed as

$$E_{an} = -K \int [\hat{n}_z^2(\vec{r}) - 1]\, d\vec{r}\,. \tag{4}$$

Consider the effect of small rotations of $\vec{M}$ from its easy axis, such that

$$\vec{M}(\vec{r}) = \vec{m}(\vec{r}) + M(1 - m^2/2M^2)\hat{z}\,, \tag{5}$$

where $\vec{m}(\vec{r})$ is a small component of the magnetization perpendicular to $\hat{z}$, the unit vector in the z direction. Then, to order m^2, the total energy E is

$$E = \sum_{\alpha} M^{-2} \int [A |\vec{\nabla} m_{\alpha}(\vec{r})|^2 + K m_{\alpha}^2(\vec{r})]\, d\vec{r}\,. \tag{6}$$

By introducing the spatial Fourier transform,

$$\vec{m}_q = \int e^{i\vec{q}\cdot\vec{r}}\, \vec{m}(\vec{r})\, d\vec{r}\,, \tag{7}$$

we obtain

$$E = \frac{\Omega}{8\pi^3 M^2} \int d\vec{q}\, m_q^2 (Aq^2 + K)\,, \tag{8}$$

where Ω is the volume of the system, and the integral is taken over the first Brillouin zone. From (8) we can identify the effective field $\vec{h}_q$, acting on $\vec{m}_q$ as

$$\vec{h}_q = (8\pi^3/\Omega)\delta E/\delta\, \vec{m}(q) = 2M^{-2}(Aq^2 + K)\vec{m}_q\,. \tag{9}$$

Inserting $\vec{h}_q$ into the torque equation for the dynamics of $\vec{m}_q$,

$$i\frac{d\vec{m}_q}{dt} = \gamma M \hat{z} \times \vec{h}_q\,, \tag{10}$$

where γ is the gyromagnetic ratio, leads to the usual dispersion relation for small q,

$$\omega_q = 2\gamma(Aq^2 + K)/M\,. \tag{11}$$

If we identify the spin-wave dispersion coefficient D by

$$\omega_q = \omega_0 + Dq^2\,, \tag{12}$$

then

$$\omega_0 = 2\gamma K/M\,, \tag{13a}$$

$$D = 2\gamma A/M. \tag{13b}$$

Thus, to calculate ω_0 and D for a disordered ferromagnet we shall need the static quantities K, M, and A, all of which are phenomenological constants to be obtained from a microscopic calculation. When the gyromagnetic ratio is also a random variable, as occurs in alloys of magnetic ions having different g values, one must replace γ by γ_{eff}, where[16]

$$\gamma_{eff} = M/\hbar S_{av}\,, \tag{14}$$

and S_{av} is the spin density, i.e., the z component of spin per unit volume. In Ref. 17 (hereafter denoted by I), we indicated that the spin-wave frequencies do not depend on the gyromagnetic ratio. For instance, in (13), γ appears only as γ/M, which by (14) is proportional to S_{av} but independent of the g value. For spins confined to a manifold of g degenerate crystal-field levels, the spin must be taken to be[18] $2S_{eff} + 1 = g$. Suitable generalizations of (14) for ferri- or antiferromagnets are also valid. For $K = 0$, the results (13) are exact as q tends to 0. When $K \neq 0$, continuum theory introduces errors, which we discuss in Sec. VI.

To describe an antiferromagnet, we introduce two directors,[13] $\hat{n}^a$ and $\hat{n}^b$, unit vectors parallel to the magnetization, i.e., the magnetic moment per unit volume, $\vec{M}$, on the two sublattices. Here, in addition to A and K, we need a third elastic constant, the exchange field H_E, to describe the stiffness for uniform rotations of one sublattice with respect to the other. As is discussed in I, the magnetostatic energy associated with small transverse fluctuations in the sublattice magnetizations $\vec{m}^a(\vec{r})$ and $\vec{m}^b(\vec{r})$ is given to order m^2 by[19]

$$E = \int \sum_{\alpha} \{(A/4M^2)|\vec{\nabla} m_{\alpha}^a(\vec{r}) - \vec{\nabla} m_{\alpha}^b(\vec{r})|^2 + (H_E/2M)[m_{\alpha}^a(\vec{r}) + m_{\alpha}^b(\vec{r})]^2 + (H_A/2M)[(m_{\alpha}^a)^2 + (m_{\alpha}^b)^2]\}\, d\vec{r}\,, \tag{15}$$

where the anisotropy field H_A is $2K/M$. As in the derivation of (9), from this expression we can evaluate effective fields which act on each Fourier component of the sublattice magnetizations. The

torque equations which result are

$$\omega m^a = \gamma M^{-1}\{[Aq^2/2 + (H_E + H_A)M]m^a + (H_E M - Aq^2/2)m^b\}, \quad (16a)$$

$$-\omega m^b = \gamma M^{-1}\{(H_E M - Aq^2/2)m^a + [Aq^2/2 + (H_E + H_A)M]m^b\}, \quad (16b)$$

and the spin-wave frequencies are found by setting the determinant of equations (16) equal to zero:

$$(\omega/\gamma)^2 = (2H_E + H_A)(H_A + Aq^2/M). \quad (17)$$

Thus, the general result for the spin-wave frequencies becomes

$$\omega = (C^2q^2 + \omega_0^2)^{1/2}, \quad (18)$$

where

$$\omega_0 = \gamma[H_A(2H_E + H_A)]^{1/2} = \gamma(4K/\chi_\perp)^{1/2} \quad (19)$$

and

$$C = \gamma[A(2H_E + H_A)/M]^{1/2} = \gamma(2A/\chi_\perp)^{1/2}, \quad (20)$$

since the perpendicular susceptibility is given by $\chi_\perp^{-1} = (H_E + \frac{1}{2}H_A)/M$. In the limit of vanishing anisotropy, the usual linear dispersion relation

$$\omega = Cq \quad (21)$$

is regained. Again the phenomenological constants M, A, H_A (or K), and H_E can only be calculated if a microscopic model is introduced. In the absence of disorder, A is found from microscopic considerations to be proportional to H_E, so that A/H_E is a geometrical constant depending only on the lattice structure and the distance dependence of the interactions. This is not true in general. We shall see below that randomness may affect these two phenomenological constants in different ways.

Finally, we consider a ferrimagnet. Our results will be used to describe disordered garnets, such as diluted YIG. For these materials we can make the simplifying assumptions that $K = 0$, and that there are only two antiferromagnetically coupled sublattices, with magnetizations $\vec{M}_a$ and $\vec{M}_b$. We shall only consider cases in which the Néel state is a good approximation to the ground state, so that we can write

$$\vec{M}_a = M_a\hat{n}^a = M_a\hat{z}, \qquad \vec{M}_b = M_b\hat{n}^b = -M_b\hat{z}. \quad (22)$$

We shall also set $\gamma_a = \gamma_b$. The generalization of (15) for small periodic fluctuations about the ordered state (22) having wave vector q and transverse amplitudes m^a and m^b on the a and b sublattices, respectively, is

$$E/\Omega = (Aq^2/4)[(m^a/M_a) - (m^b/M_b)]^2 + (\xi/2)[(m^a/M_a) + (m^b/M_b)]^2, \quad (23)$$

where ξ is a magnetic elastic constant. The equations of motion derived from (23) can be reduced, after discarding higher-order terms in q^4 and ωq^2, to the eigenvalue equation

$$(M_aM_b/\xi)(\omega/\gamma)^2 + (M_a - M_b)(\omega/\gamma) - 2Aq^2 = 0. \quad (24)$$

The factor (M_aM_b/ξ) is a generalization for ferrimagnets of $\chi_\perp$. To confirm this interpretation, we calculate the response of the system to applied magnetic fields h_x^a and h_x^b, with their relative strengths chosen to exert no net torque on the system:

$$h_a = h_0(M_b/M_a)^{1/2} \text{ on } a \text{ sites}, \quad (25a)$$

$$h_b = h_0(M_a/M_b)^{1/2} \text{ on } b \text{ sites}. \quad (25b)$$

The total energy in the presence of fields (25) and a uniform response is given by

$$E/\Omega = \tfrac{1}{2}\xi[(m^a/M_a) + (m^b/M_b)]^2 - h_am^a - h_bm^b. \quad (26)$$

The equilibrium condition, found by minimizing (26), is

$$\xi[(m^a/M_a) + (m^b/M_b)] = h_aM_a, \quad (27a)$$

$$\xi[(m^a/M_a) + (m^b/M_b)] = h_bM_b. \quad (27b)$$

These equators have a solution because $h_aM_a = h_bM_b$, by (25). To define $\chi_\perp$ for the ferrimagnet, we require that

$$E/\Omega = -\tfrac{1}{2}h_0^2\chi_\perp. \quad (28)$$

Equation (27) is sufficient to determine E, even though m^a and m^b are determined only up to a net rotation of all of the spins. Substituting into (28), we identify

$$\chi_\perp = M_aM_b/\xi. \quad (29)$$

There is an alternate expression for $\chi_\perp$, which proves more convenient for microscopic calculation. We consider that part of the response which does not involve a rotation of the staggered magnetization, i.e., we require $m^a = m^b$. Then (27) implies

$$m^a = m^b = (h_aM_a/\xi)/(M_a^{-1} + M_b^{-1}). \quad (30)$$

We then find that $\chi_\perp$ is equal to the ratio of the response to a weighted average of the applied fields:

$$\chi_\perp = (m^a + m^b)(M_a + M_b)/(h_aM_a + h_bM_b). \quad (31)$$

With either definition of $\chi_\perp$, the eigenfrequency

equation becomes

$$\chi_\perp(\omega/\gamma)^2+(M_a-M_b)(\omega/\gamma)-2Aq^2=0\,. \tag{32}$$

Just as was pointed out in connection with (13), the spin-wave frequencies given by Eq. (32) do not depend upon g values since $\chi_\perp \propto \gamma^2$. This point has been discussed in greater detail in I. In the limit $M_a=M_b=M$ we recover from (32) the antiferromagnetic result, (21). When M_a is not equal to M_b, the lowest mode frequency is proportional to q^2, and is given by (11), with $K=0$. The second solution of (32) describes an optical mode. Its frequency at $q=0$, is

$$\omega_{\rm opt}=\gamma|M_a-M_b|/\chi_\perp\,. \tag{33}$$

As we shall see in Sec. X, our definition of $\chi_\perp$ for the ferrimagnet, together with (33), reproduces the well-known result of Kaplan and Kittel[16,20] for the two-sublattice ferrimagnet. We note that $\omega_{\rm opt}$ becomes small near compensation, or whenever $\chi_\perp$ is large. When $\omega_{\rm opt}$ becomes small, the acoustic branch of excitations exhibits both q and q^2 dependences, since the solution to (32),

$$\omega=[(\tfrac{1}{2}\omega_{\rm opt})^2+2A\gamma^2q^2/\chi_\perp]^{1/2}-\tfrac{1}{2}\omega_{\rm opt}\,, \tag{34}$$

can be approximated by

$$\omega\sim\gamma(2A/\chi_\perp)^{1/2}q-\tfrac{1}{2}\omega_{\rm opt}\,, \tag{35}$$

when $q^2\gg q_c^2$, where

$$q_c^2=(M_a-M_b)^2/8A\chi_\perp\,. \tag{36}$$

In the opposite limit, $q\ll q_c$, (11) holds.

This derivation is most reliable as $\omega_{\rm opt}$ tends to zero. As $\omega_{\rm opt}$ increases (e.g., when M_a-M_b is changed by varying the concentration), the continuum picture becomes less appropriate. The optical mode formed in one region no longer has the same energy as that in other regions. Thus we expect this optical mode to develop a width. In addition, the mean frequency of the optical mode can differ from the prediction of (33), since the modes with $\omega<\omega_{\rm opt}$ will not have time to continuously relax to equilibrium during each cycle of the optical mode. To take account of this effect, $\chi_\perp$ in (33) should be taken to be not the static susceptibility, but rather $\chi_\perp(\omega=\omega_{\rm opt})$.

IV. MICROSCOPIC THEORY FOR STATIC PROPERTIES

In this section we describe the way the static parameters necessary for the evaluation of ω_q can be determined from linear response theory. This will be done by a direct numerical evaluation of the linear response of the system as described microscopically. The microscopic calculations will be performed in the limit $T\to0$, assuming the spins to be classical. As is well known, the classical limit gives the correct behavior for a quantum spin system in the limit $S\to\infty$. Thus, for quantum systems, our results should be valid to leading order in $1/S$.

We first consider the ferromagnet. In the presence of an applied field

$$\vec{h}(x,y,z)=h_0(\hat{x}\cos qx+\hat{y}\sin qx)\,, \tag{37}$$

a magnetization

$$\vec{m}(x,y,z)=m_\perp(\hat{x}\cos qx+\hat{y}\sin qx) \tag{38}$$

is induced. To determine $m_\perp$ we use the continuum description (6) for the total energy:

$$E_{\rm tot}/\Omega=(Aq^2+K)m_\perp^2/M^2-h_0m_\perp\,. \tag{39}$$

Therefore, at equilibrium

$$m_\perp/h_0=\tfrac{1}{2}M^2(Aq^2+K)^{-1}=\chi_q \tag{40}$$

and

$$E_{\rm tot}/\Omega=-\tfrac{1}{4}M^2h_0^2(Aq^2+K)^{-1}$$
$$=-\tfrac{1}{2}\chi_qh_0^2\,. \tag{41}$$

Accordingly, a microscopic calculation of $m_\perp/h_0$ or $E_{\rm tot}$ will enable us to determine A and K. In the case of dilution, A and K depend upon the concentration p of magnetic sites. In doing these calculations, we recognize that any finite-sized cluster will have zero magnetization for $T>0$. Hence, $M(p)$ is identified as $M(1)P(p)$, where $P(p)$ is the fraction of sites not in a finite cluster.[14]

Microscopically, $m_\perp$ is calculated from the equilibrium orientations of the spins, S_i, which are in turn determined by minimizing the microscopic energy, $e_{\rm tot}$. Since isolated clusters of occupied sites do not contribute to the collective behavior, we neglect them in writing the following expression for $e_{\rm tot}$:

$$e_{\rm tot}=-2J\sum_{i,j}p_ip_j\vec{S}_i\cdot\vec{S}_j-\sum_i\Delta_ip_iS_1^z$$
$$-g\mu_B\sum_i\vec{S}_i\cdot\vec{h}_ip_i\,. \tag{42}$$

Here, p_i is unity if i is an occupied site in the infinite cluster, and is zero otherwise, and i and j are pairs of nearest-neighbor lattice sites. For small deviations from equilibrium, we set

$$\vec{S}_i=S[(1-\tfrac{1}{2}\theta_i^2)\hat{z}+\theta_i\hat{n}_i]\,, \tag{43}$$

with $\hat{n}_i$ a unit vector parallel to $\vec{h}_i$. Then the equilibrium conditions can be written as

$$2JS^2\sum_j p_ip_j(\theta_i-\theta_j)\hat{n}_i+p_i\Delta_iS\theta_i\hat{n}_i=g\mu_BS\vec{h}_ip_i\,. \tag{44}$$

Combining this equation with (42) we have

$$e_{\rm tot}=-\frac{g\mu_BS}{2}\sum_i p_i\theta_ih_i\,, \tag{45}$$

where θ_i is the solution to (44).

To determine the macroscopic parameters we proceed as follows. We first determine $M(p)$ by calculating the percolation concentration $P(p)$, which is defined so that $P(p)$ is the probability that a site is in the infinite cluster. Then we have $M(p)/M^0 = P(p)$, where M^0 denotes $M(1) = g\mu_B \sum_i S_i^z/\Omega$. To determine $K(p)$ we evaluate $e_{\rm tot}$ for $q=0$ and equate the result to $E_{\rm tot}$ given in (41). Finally, to determine $A(p)$, we evaluate $e_{\rm tot}$ for small q and compare the result with $E_{\rm tot}$ in (41) using the above-determined value of $K(p)$.

In the absence of anisotropy, a simpler configuration can be used to calculate $A(p)$. For this purpose we consider (44) for a system obeying periodic boundary conditions in the y and z directions, but having surfaces at $x=a$ and $x=La$. For the case $h(r)=0$, but with the boundary conditions $\theta_i=\theta^0$ for $x=La$ and $\theta_i=-\theta^0$ for $x=a$, (43) becomes equivalent to Kirchoff's law for a network of conductances $\sigma_{ij}=2JS^2p_ip_j$ connecting electrodes of potentials θ^0 and $-\theta^0$. Then one has the relation

$$\sigma(p)/\sigma(1)=A(p)/A(1), \tag{46}$$

given previously by Brenig *et al.*[21] and by Kirkpatrick.[22] The constant-voltage boundary condition is equivalent to fixing the directions of the spins on two edges of the sample. For an anisotropic system this boundary condition induces large angles between spins near the edges, and is thus outside the domain of continuum theory. For such systems, the stiffness $A(p)$ must be extracted from (41).

We now discuss the situation for the dilute ferrimagnet, and for simplicity set $K=0$. As will be seen, the dilute antiferromagnet can usefully be considered as the special case when the system has no net moment. Referring to (24) we see that it is necessary to determine $A(p)$ and $\chi_\perp(p)$. The determination of $A(p)$ proceeds as for the ferromagnet. For a multisublattice structure we write

$$S_i = S_i^z[(1-\tfrac{1}{2}\theta_i^2)\hat{z}+\theta_i\hat{n}], \tag{47}$$

where S_i^z is evaluated in the Néel state: $S_i^z=\pm S_i$, where S_i is the magnitude of the spin at i. Then, in the absence of anisotropy and applied field, the equilibrium condition is

$$\sum_j 2J_{ij}S_i^zS_j^zp_ip_j(\theta_i-\theta_j)=0. \tag{48}$$

In analogy with the single-sublattice case, we see that (48) is equivalent to Kirchoff's law for a network with conductances

$$\sigma_{ij}=2p_ip_jJ_{ij}S_i^zS_j^z. \tag{49}$$

As in the ferromagnetic case, $A(p)/A(1) = \sigma(p)/\sigma(1)$, where $\sigma(p)$ is the conductivity of the network of (49). In fact, since the σ's for a ferromagnet and an antiferromagnet are the same if the crystal lattices are the same, one sees that the A's for the two systems are identical.

Finally we describe the microscope evaluation of $\chi_\perp(p)$. For this purpose we apply the torque-free field (25). For simplicity, we describe the treatment of the case where all spins have a common magnitude S. We write

$$\vec{S}_i = S_i^z(1-\tfrac{1}{2}\theta_i^2)\hat{z}+S\theta_i\hat{n}, \tag{50}$$

with $\hat{n}$ parallel to $\vec{h}_i=h_i\hat{x}$. Then the equilibrium conditions are

$$\sum_j 2J_{ij}(S_i^zS_j^z\theta_i - S^2\theta_j) = g\mu_B h_0 S\psi^{-1/2} \quad (i \text{ on the } a \text{ sublattice}), \tag{51a}$$

$$\sum_j 2J_{ij}(S_i^zS_j^z\theta_i - S^2\theta_j) = g\mu_B h_0 S\psi^{1/2} \quad (i \text{ on the } b \text{ sublattice}), \tag{51b}$$

where ψ is defined as

$$\psi = N^a/N^b, \tag{52}$$

where N^μ is the number of sites in the infinite cluster which are in the μ sublattice.

Finite clusters will also contribute to $\chi_\perp$. At low temperatures, the effect of clusters of zero net spin can be neglected for $p>p_c$, but clusters containing an odd number of sites will give rise to contributions $\propto 1/T$, which can become large at low temperatures. This temperature dependance can be used to separate out cluster effects from a measured static susceptibility. Since neither type of finite-cluster contribution affects spin dynamics at long wavelengths, and both are regular functions of p at the percolation threshold, we shall need to consider only the infinite cluster in the remainder of this paper.[23] (See, however, the discussion of static susceptibility measurements in Sec. IX.)

Note that θ^0, where

$$\theta_i^0 = 1 \quad (\text{on the } a \text{ sublattice}), \tag{53a}$$

$$\theta_i^0 = -1 \quad (\text{on the } b \text{ sublattice}), \tag{53b}$$

solves the homogeneous version of (51). Presumably this solution is the only one for $h_0=0$ which has nonzero amplitude in the infinite cluster. Since the right-hand side (51) is orthogonal to θ^0, a solution to (51) does exist. Also, we use orthogonality to the homogeneous solution to require that

$$\sum_{a \text{ sublattice}} \theta_i = \sum_{b \text{ sublattice}} \theta_i, \tag{54}$$

which means that $m^a=m^b$. So the solution to (51) under the constraint (54) describes the torque-free response to the torque-free applied field. Using the

solution to (51) we find that

$$\chi_\perp = \sum_i p_i(\theta_i/h_0)(g\mu_B S/\Omega)[\tfrac{1}{2}(\psi^{1/2}+\psi^{-1/2})]. \quad (55)$$

For the dilute antiferromagnet we also use this formula. Here, as the sample size increases, $\psi \to 1$. However, in practice for finite samples in which fluctuations in the dilution of the two sublattices occurs, $N_a \neq N_b$ and the formulation we give here is helpful. To treat the case of an antiferromagnet with $K \neq 0$, one can use methods similar to those described above for a ferromagnet. (For an example, see I.)

V. SOLUBLE MODELS

In this section we give a number of exact analytic results for random linear systems. Dilution in 1D cuts a chain into finite segments and destroys long-wave length modes, but collective modes can persist in the presence of fluctuations in the value of J_{ij} about some average, as is believed to occur in the polymer antiferromagnetic poly-(metal phosphinate)s.[24,25] From the resistor-network analogy, a magnetic chain is identified as a series network. Its resistivity is obtained by averaging the individual resistances. Thus,

$$\langle A(\{J_{ij}\})\rangle \propto \langle |J_{ij}S_iS_j|^{-1}\rangle^{-1}, \quad (56)$$

where the average in (56), indicated by $\langle\ \rangle$, is taken over the distribution of the set $\{J_{ij}\}$ of bonds. This presecription holds even when the signs of J fluctuate, since a ground state can still be constructed by fixing the orientation of the spin S_0 at one end of the chain and, working along the chain, choosing the sign of each S_i^z to make $J_{i-1,i}S_{i-1}^zS_i^z$ positive. One can view a 1D chain as the limiting case opposite to average-medium theory, in the following sense. In such a theory one averages over conductances as in a parallel circuit, thereby minimizing the interactions between statistical fluctuations, so that

$$\langle A(\{J_{ij}\})\rangle = A(\{\langle J_{ij}\rangle\}). \quad (57)$$

In contrast, the exact result for a linear system with nearest-neighbor interactions only is given by (56), and is the result for resistors in series. These series and parallel situations form bounds between which the realistic 2D and 3D cases will fall.

An exact result for the perpendicular susceptibility is also easily obtained for a linear antiferromagnetic chain in which the magnitude of J_{ij} is a random variable, but the signs are fixed and $|S_i^z| \equiv S$ is constant. We confine our attention to systems with only nearest-neighbor interactions and write $J_{n,n+1} \equiv J_n$, $J_{N,1} \equiv J_N$ for a chain of N spins (N even). Here we will study the case of free ends, $J_N = 0$. (In Appendix B we treat the case $J_N \neq 0$.) The equations for the spin deviations induced by a uniform external field, $h\hat{x}$, can be written in the form

$$e_{i-1} + e_i = h, \quad (58)$$

where

$$e_i = 2J_i(S_i^x + S_{i+1}^x) \quad \text{for } 1 \leq i \leq N,$$
$$e_N = e_0 = 0. \quad (59)$$

Subtracting the first such equation from the second, then the second equation from the third, and so forth, gives

$$e_i = h \ \ (i \text{ odd}), \quad e_i = 0 \ \ (i \text{ even}). \quad (60)$$

Dividing each of Eqs. (60) by J_i and adding them yields

$$\chi_\perp = (2N)^{-1}\sum_{i\ \text{odd}}(2J_i)^{-1}. \quad (61)$$

Since $\chi_\perp$ is a linear function of J_i^{-1} one can express the configurationally averaged $\chi_\perp$ as

$$\langle\chi_\perp(\{J_i\})\rangle = \chi_\perp(\{\langle J_i^{-1}\rangle^{-1}\}). \quad (62)$$

A complete solution of the general case, with no restrictions on the sign of J or size of the S_i, is obtained by first solving[26,27]

$$\sum_j D_{ij}\chi_{jk} = \delta_{ik} - \varphi_i^0\varphi_k^0,$$

with (63)

$$\sum_j \chi_{jk}\varphi_j^0 = 0,$$

where D_{ij} is the dynamical matrix,

$$D_{ij} = \sum_k 2|J_{ik}|[(S_k/S_i)\delta_{ij} - \delta_{jk}\xi_j\xi_k]. \quad (64)$$

In (64) the spin direction $\xi_j \equiv \langle S_j^z\rangle/S_j = \pm 1$ is assigned with the convention $\xi_1 = +1$, and φ^0 is the eigenvector of $\underline{D}$ corresponding to uniform spin rotation: $\varphi_i^0 = \xi_i S_i/(\sum_j S_j^2)^{1/2}$ so that $\underline{D}\varphi^0 = 0$. We consider an ensemble of J's such that $\prod_{i=1}^N J_i \geq 0$, so that a ground state can be constructed in which $J_i\xi_i\xi_{i+1} \geq 0$ for every i. For a chain with free ends (i.e., $J_N = 0$) the susceptibility, $\chi^0(i,j)$, is

$$\chi^0(i,j) = \left(\sum_{k=1}^{i-1}\sigma_k^{-1}T_k^2 - \sum_{k=1}^{j-1}\sigma_k^{-1}T_kU_k + \sum_{k=j}^{N-1}\sigma_k^{-1}U_k^2\right) \times\left(\frac{\xi_i\xi_jS_iS_j}{(NS_{\text{av}}^2)^2}\right), \quad i \leq j \quad (65a)$$

$$\chi^0(j,i) = \chi^0(i,j), \quad (65b)$$

where

$$T_j = \sum_{k=1}^{j} S_k^2, \quad (66a)$$

$$U_j = \sum_{k=j+1}^{N} S_k^2 , \tag{66b}$$

$$S_{av}^2 = (T_j + U_j)/N , \tag{66c}$$

$$\sigma_j = |2J_j S_j S_{j+1}| . \tag{66d}$$

When ξ_i and S_i are constant, the general solution simplifies. Then only σ_i is random and one has a generalization of (62):

$$\langle \chi^0(i,j) \rangle = \chi^0(i,j; J_k = \langle J_k^{-1} \rangle^{-1}) . \tag{67}$$

Since $\chi(q) \sim S^2/A(q-Q)^2$ for $q \to Q$, where $Q=0$ for a ferromagnet and $Q=\pi/a$ for an antiferromagnet, this also provides a quick but restricted derivation of (56).

We may apply (62) to the poly-(metal phosphinate)s. Following Scott *et al.*[24] we assume each J_i to be randomly distributed as

$$P(J) = \begin{cases} (2\lambda J_0)^{-1}, & -J_0(1+\lambda) \le J \le -J_0(1-\lambda) \quad (68a) \\ 0, \quad \text{otherwise.} & (68b) \end{cases}$$

This leads to the result

$$\langle J^{-1} \rangle^{-1} = 2\lambda J_0 [\ln(1+\lambda)/(1-\lambda)]^{-1} . \tag{69}$$

Thus $A \to 0$ as $\lambda \to 1$, according to (56), and also

$$\chi q(\lambda) = [\ln(1+\lambda)/(1-\lambda)]\chi_q(0)/2\lambda \tag{70a}$$

$$= \{[\ln(1+\lambda)/(1-\lambda)]/2\lambda\}/4J_0(1-\cos qa) , \tag{70b}$$

where a is the lattice spacing. Indeed, Scott *et al.*[24] do observe an increase and a divergence in χ^0 as the disorder is increased. At present, however, the experimental correlation between disorder and increased susceptibility is only qualitative.

The above authors have also considered the case when the distribution of J's stretches through zero. It is clear that unless $P(J) \to 0$ as $J \to 0$ that

$$\langle |J|^{-1} \rangle = \int J^{-1}[P(J) + P(-J)]\, dJ \tag{71}$$

diverges, and therefore, that $A = 0$.

It is interesting to consider a model in which each J fluctuates in sign but not in magnitude. Let p be the concentration of negative J's. Then (56) implies that $A(p) = A(0)$ independent of p.

VI. EXACT RESULTS FOR A SINGLE VACANCY

In this section we present the exact results for the case of a single vacancy. This will enable us to obtain the corrections to various quantities correct to first order in the vacancy concentration, $c = 1-p$. Initially, we shall consider isotropic systems. We then discuss quantitatively the effects of anisotropy in order to assess the validity of continuum theory for the dynamics of such systems.

First we calculate the conductivity of a network with a single vacancy. To do this we solve the circuit equations for a random network with periodic boundary conditions in the y and z directions, and with sites on the surfaces at $x=0$ and $L+1$ kept at potentials $-V_0$ and V_0, respectively. For cubic symmetry the conductivity σ, which in general is a second-rank tensor, becomes scalar, so for convenience we have taken the potential gradient to lie along a crystal axis. Also, for simplicity, we consider initially a simple cubic lattice of unit lattice constant.

For sites i which are not on the surface and which have no neighbors on the surface, Kirchoff's equation are

$$\sum_d p_i p_{i+d}(V_i - V_{i+d}) = 0 , \tag{72a}$$

where in general d will denote one of the possible vectors joining a site to its nearest neighbors. For sites with neighbors on the surface, we write

$$\sum_d p_i p_{i+d}(V_i - \xi_{i+d} V_{i+d}) = \sum_d p_i p_{i+d}(1-\xi_{i+d}) V_{i+d} , \tag{72b}$$

where $\xi_i = 0$ if i is on the surface, and the surface voltages are given to be $\pm V_0$. These equations are of the form

$$\underline{N} V = \varphi , \tag{73}$$

where φ represents the surface voltage terms on the right-hand side of (72b). For the pure system $\underline{N} = \underline{N}_0$, where

$$(\underline{N}_0)_{ij} = [4/L^2(L+1)] \sum_{k,q,q'} \exp[iq(y_i - y_j)] \exp[iq'(z_i - z_j)] \sin kx_i \sin kx_j (3 - \cos k - \cos q - \cos q') , \tag{74}$$

where $\vec{r}_i = (x_i, y_i, z_i)$ is the position of the site i, L is the number of interior sites along the x, y, or z directions in the sample, k is summed over the values $\pi r/(L+1)$, and q and q' are summed over the values $2\pi s/L$ (r and s are integers with $1 \le r, s \le L$). The basis functions $[2/(L+1)]^{1/2} \times \sin kx$ incorporate the free surface boundary conditions of $\underline{N}_0$. We take L to be an odd integer.

In the presence of a single vacancy at site k, N_{ij} is modified whenever i or j is within one site of k. In such cases, (72) reads

$$\sum_{d' \ne d} (V_{k+d} - V_{k+d-d'}) = 0 , \tag{75}$$

and V_k is arbitrary.

Since the response to a vacancy is local, its exact position is immaterial. We shall place it in the center plane of the sample. To find the effect on σ of a single vacancy at $\vec{r}_0 = (L+1)/2\,\hat{x}$ we solve

$$\underline{N}\,V \equiv (\underline{N}_0 + \delta\underline{N})V = \varphi\,, \tag{76}$$

with

$$\delta N_{ij} = -\sum_d (\delta_{i,0} - \delta_{i,0+d})(\delta_{j,0} - \delta_{j,0+d})\,. \tag{77}$$

where $\delta_{i,j} = 1$ if and only if $r_i = r_j$. Thus

$$V = \underline{N}^{-1}\varphi = \underline{N}_0^{-1}\varphi + \underline{N}_0^{-1}\,\underline{t}\,\underline{N}_0^{-1}\varphi\,, \tag{78}$$

where

$$\underline{t} = -\delta\underline{N}(1 + \underline{N}_0^{-1}\delta\underline{N})^{-1} \tag{79}$$

is the single vacancy t matrix.[28,29] Strictly speaking, $\underline{N}^{-1}$ does not exist because $\underline{N}\,|\psi_0\rangle = 0$, where $|\psi_0\rangle$ is an excitation on the vacant site. However, since $\underline{N}^{-1}$ operates on φ, which is orthogonal to $|\psi_0\rangle$, this difficulty does not arise. To remove this formal problem we will replace $\underline{N}$ by $\underline{N} - \omega$, so that $-\underline{N}(\omega)^{-1}$ is the dynamic Green's function. At the end of the calculation we shall set $\omega = 0$. Similarly, we could introduce $\underline{N}_0(\omega) = \underline{N}_0 - \omega$. From (74) it is clear that $\underline{N}_0$ does not have a zero eigenvalue since for our set of boundary conditions k is never zero. Consequently, the limit $\omega \to 0$ can be taken in $\underline{N}_0$ at the beginning of the calculation. However, since $t(\omega)$ is singular for $\omega = 0$ we must retain its frequency dependence until the end of the calculation.[30]

Let $\psi(r)$ take the values 1 for $x = \frac{1}{2}(L+3)$ and -1 for $x = \frac{1}{2}(L-1)$. Then the conductivity is given by

$$2V_0 - \langle\psi|\,V\rangle/L^2 = 2[(L-1)/(L+1)]\,V_0\,\sigma/\sigma_{\text{pure}}\,. \tag{80}$$

We now use (78) noting that

$$\langle\psi|\,\underline{N}_0^{-1}\,|\varphi\rangle = 4L^2V_0/(L+1)\,, \tag{81}$$

so that (80) becomes

$$\sigma/\sigma_{\text{pure}} = 1 - [(L+1)/2L^2V_0(L-1)]\langle\psi|\,\underline{N}_0^{-1}t(\omega)\underline{N}_0^{-1}\,|\varphi\rangle \quad \text{as } \omega \to 0\,. \tag{82}$$

Only the p-wave part of the t matrix is involved here, since both $|\psi\rangle$ and $|\varphi\rangle$ are odd functions of x, and even functions of y and z. A detailed calculation shows that for large L

$$\sigma/\sigma_{\text{pure}} = 1 - 2t_p/N\,. \tag{83}$$

Here N is the number of sites, and t_p is the p-wave t matrix defined by

$$t_p = \frac{1}{2}\sum_{m,n=\pm1} mn\,t(m + \tfrac{1}{2}(L+1), n + \tfrac{1}{2}(L+1))\,, \tag{84}$$

and is given explicitly as $t_p = t_p(0)$, where

$$t_p(\omega) = [1 - I(\omega)]^{-1}\,, \tag{85}$$

and

$$I(\omega) = \frac{2}{Nz}\sum_k \frac{\sin^2 k_x a}{(1-\gamma_k) - \omega}\,, \tag{86}$$

where $\gamma_k = z^{-1}\sum_d e^{ikd}$. Thus for a low concentration c of vacancies, we obtain

$$\sigma(c)/\sigma(0) = 1 - 2ct_p\,. \tag{87}$$

This formula is easily generalized to other lattices by expressing (86) as

$$I(\omega) = (Nz)^{-1}\sum_k |\varphi_{px}(k)|^2/[(1-\gamma_k) - \omega]\,, \tag{88}$$

where for the square and cubic lattices:

$$\varphi_{px}(k) = 2^{1/2}\sin k_x a \quad \text{(sq, sc)} \tag{89a}$$

$$= 8^{1/2}\sin(\tfrac{1}{2}k_x a)\cos(\tfrac{1}{2}k_y a)\cos(\tfrac{1}{2}k_z a) \quad \text{(bcc)} \tag{89b}$$

$$= 2^{1/2}\sin(\tfrac{1}{2}k_x a)[\cos(\tfrac{1}{2}k_y a) + \cos(\tfrac{1}{2}k_z a)] \quad \text{(fcc)}. \tag{89c}$$

For the dilute ferromagnet, Izyumov[28] has previously derived the result

$$D(c)/D(0) = 1 - 2c\,t_p + c\,. \tag{90}$$

Since $M(c)/M(0) = 1 - c$, and $D \propto A/M$, (90) is equivalent to (87). We can make an estimate of t_p for use on more complicated lattices by observing that $I(0) \sim z^{-1}$ in (86) when z is reasonably large. Substituting this approximation into (85) we find

$$t_p \sim 1 + (z-1)^{-1}\,. \tag{91}$$

For the sc lattice, for example, (91) gives $t_p \sim 1.2$, in reasonable agreement with the exact result, ~ 1.26. Other values of t_p are given in Table I, where one finds that (91) is qualitatively correct.

Next we calculate the static magnetic elastic constants in the presence of anisotropy, correct to first order in c. We can then compare known results for $D(c)/D(0)$ with the quantity $[A(c)/A(0)]/[M(c)/M(0)]$, in order to see how important are finite frequency corrections to the zero-frequency result $D \propto A/M$. As one might expect, these corrections are found to be of order ω_0/ω_E, where

TABLE I. Useful matrix elements for common lattices.

Lattice	t_p	$1 + (z-1)^{-1}$	P_0
sq	1.57	1.33	···
sc	1.265	1.20	−1.51
bcc	1.19	1.14	−1.49
fcc	1.15	1.09	···

ω_0 is the frequency of the anisotropy gap.

To treat the anisotropic case we solve (44) exactly for the equilibrium angles θ_r in the presence of a single vacancy using the t matrix, as above. We then evaluate the total energy $e_{\rm tot}$ according to (45) using the solution for θ_r. In this way we obtain the result

$$e_{\rm tot}/h^2 = -(M^2\Omega/4)/(K_0 + JS^2q^2/a) + g^2\mu_B^2 S^2/4K_0 v - \frac{2JSa^2q^2g^2\mu_B^2 S t_p(-\eta)}{[2JzS(1-\gamma_q)+(2K_0 v/S)]^2}, \quad (92)$$

where v is the volume per site, $K_0 = (S\Delta/2v) = K(c=0)$, and $\eta = 2K_0 v/2JzS^2$. For $q=0$ we have

$$e_{\rm tot}/h^2 = -M_0^2\Omega(1-N^{-1})/4K_0 . \quad (93)$$

For Nc vacancies with $c \ll 1$ we replace $(1-N^{-1})$ by $1-c$. Then, to lowest order in c,

$$e_{\rm tot} = -(\tfrac{1}{4}h^2)(1-c)^2 M_0^2\Omega/(1-c)K_0 . \quad (94)$$

Since we know that $M(c) = (1-c)M_0$, comparison of this form with (41) shows that

$$K(c) = (1-c)K_0 . \quad (95)$$

This is expected, since $H_A(c) = 2K(c)/M(c)$ is independent of c as long as Δ is independent of c. A similar analysis of the q-dependent contributions to $e_{\rm tot}$ leads to the result

$$A(c, K_0) = A(0,0)[1 - 2ct_p(-\eta)] . \quad (96)$$

This is the correct result for the static elastic constant $A(c)$ for nonzero K_0.

However, when $K_0 \neq 0$,

$$D(c,K) \neq D_{\rm static}(c,K) , \quad (97)$$

where $D_{\rm static}$ is defined by

$$D_{\rm static}(c,K) \equiv 2\gamma A(c,K)/M(c) . \quad (98)$$

To see this we note that anisotropy uniformly shifts the single spin-wave states upwards in energy by an amount

$$h\omega_0 = \Delta = 2K_0 v/S . \quad (99)$$

Thus,

$$\omega_q(c) = 2K_0 v/\hbar S + D(c, K=0)q^2 , \quad (100)$$

and the correct result is $D(c,K) = D(c,0)$. In contrast, static continuum theory would have given

$$\omega_q(c) = 2g\mu_B K(c)/\hbar M(c) + D_{\rm static}(c,K)q^2 . \quad (101)$$

Comparing these results, we see that the gap frequency is the same in both cases, but the value of D is different. In (100), which is the correct result, we use the value of $A(c)$ calculated for $\omega = \omega_q \sim \omega_0$, i.e., on resonance, whereas it is incorrect to use the static value of A in the relation $D = A/M$. Since we know the frequency dependence of $A(c)$ is embodied in $t_p(\eta)$, we can see exactly how large an error is made in (100) by taking the static ($\eta = 2Kv/2JzS^2$) value rather than the on-resonance ($\eta = 0$) value. From (85) we have for $\eta \ll 1$

$$t_p(\eta) \sim t_p(0) + \eta\, t_p(0)^2 \frac{dI(0)}{d\eta} , \quad (102)$$

with

$$\frac{dI(0)}{d\eta} = -\frac{2}{Nz}\sum_k \sin^2 k_x a(1-\gamma_k)^{-2} = -0.36 , \quad (103)$$

so that

$$t_p(\eta) = t_p(0)(1 - 0.48\eta) . \quad (104)$$

For reasonably small anisotropy, i.e., for $\eta = 2Kv/2zJS^2 = \hbar\omega_0/2zJS \sim 0.1$, the difference between $t_p(\eta)$ and $t_p(0)$ is only a 5% effect.

We now perform the same analysis within the low-concentration theory for the antiferromagnet[31-33] by (i) calculating the magnetic elastic constants in the presence of anisotropy, (ii) developing expressions for the spin-wave dispersion relation based on a dynamic calculation, and (iii) comparing the results of (ii) with the continuum results, which are rigorous only in the zero-anisotropy limit. As for the ferromagnet, we find that the discrepancies between the static and dynamic results are of order ω_0/ω_E. The two-dimensional case is somewhat special, and is discussed separately below.

The low-concentration expressions for the static response functions were given in I, and are collected here for convenience:

$$A^{-1}\frac{dA}{dc} = -2\,t_p(-\eta) , \quad (105a)$$

$$K^{-1}\frac{dK}{dc} = -1 , \quad (105b)$$

$$\chi^{-1}\frac{d\chi}{dc} = -\frac{4+\delta_A+P_0(0)(1+\delta_A)(\delta_A+2)^2}{(\delta_A+2)[1+\delta_A(1+\delta_A)P_0(0)]} , \quad (105c)$$

where $\delta_A = \omega_A/\omega_E$ and $P_0(\omega) = N^{-1}\sum_q \omega_E^2/(\omega^2 - \omega_q^2)$. $P_0(0)$ is given for the appropriate lattices in Table I. Note that for classical spin systems, A and K are invariant under the change of sign, $J \to -J$. Hence (105a) and (105b) are identical to the results for a ferromagnet on the same crystal lattice.

The dynamic calculation at low concentration involves evaluation of the self-energy $\Sigma(q,\omega)$ defined by

$$\chi(q,\omega) = [\omega_A + \omega_E(1-\gamma_q)]/[\omega^2 - \omega_q^2 - c\Sigma(q,\omega)] . \quad (106)$$

Since the analysis is similar to that in Appendix B of I, we give only the result:

$$\Sigma(q,\omega)=A_{-1}(\omega)/2[\omega_A+\omega_E(1-\gamma_q)]\,, \tag{107}$$

where $A_{-1}(\omega)$ is given in Eq. (B7) of I. The spin-wave energies of the dilute system are expressed in terms of Σ by

$$\omega_q^2(c)=\omega_q^2+c\Sigma(q,\omega_q)\,. \tag{108}$$

We find that[34]

$$\Sigma(q,\omega_q)=\frac{2\{(1+\delta_A-\gamma_q^2)[1-(1+\delta_A-\gamma_q^2)P_0(\omega_q)]\omega_E^2+\omega_q^2P_0(\omega_q)\}}{[1-(1+\delta_A-\gamma_q^2)P_0(\omega_q)]^2-[\omega_qP_0(\omega_q)/\omega_E]^2}$$

$$-\sum_{\alpha\neq s}|\langle q|\varphi_\alpha\rangle|^2[(\omega_E+\omega_A-\omega_q)t_\alpha(\omega_q)+(\omega_E+\omega_A+\omega_q)t_\alpha(-\omega_q)]/\hbar\,, \tag{109}$$

where t_α is the t matrix for the symmetry label, $\alpha=p$ or d, and $|\varphi_\alpha\rangle$ is an associated basis function, e.g., $\langle q|\varphi_{px}\rangle=2^{1/2}\sin q_x a$ for an sc lattice. From continuum theory we would expect

$$-\omega_0^{-2}\frac{d\omega_0^2}{dc}=-K^{-1}\frac{dK}{dc}+\chi_\perp^{-1}d\chi_\perp/dc\equiv\alpha_{\text{static}}\,, \tag{110a}$$

$$\lim_{q\to0}-(\omega_q^2-\omega_0^2)^{-1}\frac{d(\omega_q^2-\omega_0^2)}{dc}=-A^{-1}\frac{dA}{dc}+\chi_\perp^{-1}\frac{d\chi_\perp}{dc}$$

$$\equiv\beta_{\text{static}}\,. \tag{110b}$$

The correct results follow from the dynamical calculation:

$$-\omega_0^{-2}\frac{d\omega_0^2}{dc}=-\omega_0^{-2}\Sigma(0,\omega_0)\equiv\alpha_{\text{dynamic}}\,,$$

$$\lim_{q\to0}-(\omega_q^2-\omega_0^2)^{-1}\frac{d(\omega_q^2-\omega_0^2)}{dc} \tag{111}$$

$$=\lim_{q\to0}(1-\gamma_q^2)^{-1}\omega_E^{-2}[\Sigma(0,\omega_0)-\Sigma(q,\omega_q)]\equiv\beta_{\text{dynamic}}\,.$$

The dominant contribution to the difference between the static and dynamic results is of order ω_0/ω_E, and results from the frequency dependence of P_0:

$$P_0(0)-P_0(\omega_0)\sim(2b)^{3/2}\omega_0/(4\pi\omega_E),\quad \omega_0\ll\omega_E \tag{112}$$

where b is the constant defined for a given lattice by $\gamma_q\sim1-ba^2q^2$. Using (109) we find

$$\alpha_{\text{dynamic}}-\alpha_{\text{static}}\sim(2b)^{-3/2}\omega_0/2\pi\omega_E\,, \tag{113a}$$

$$\beta_{\text{dynamic}}-\beta_{\text{static}}\sim(2b)^{-3/2}\omega_0/2\pi\omega_E\,. \tag{113b}$$

Both quantities are positive, and of order ω_0/ω_E, just as for the ferromagnet. For example, consider MnF_2, where $b=\frac{1}{8}$ and[35] $\omega_0/\omega_E=0.17$. According to (110)–(113) the initial slope $-\omega_q^{-1}d\omega_q/dc$ calculated using the static elastic constants is about 10% less than the exact result given by low-concentration theory. Most of the "ideal" magnetic materials which have been studied[36] are less anisotropic than MnF_2, and thus should show smaller discrepancies.

Finally, we consider $\chi_\perp$ for two-dimensional lattices. Here P_0 depends upon the shape of the sample and diverges in the limit $N\to\infty$. For a simple square lattice the result is

$$P_0=\pi^{-1}\ln N+\tfrac{1}{3}x-\pi^{-1}\ln(x/2\pi^2)+2\gamma/\pi$$

$$+\frac{4}{\pi}\sum_n{}'n^{-1}(e^{2\pi nx}-1)^{-1}\,, \tag{114}$$

where $\gamma\sim0.577$ is Euler's constant, x is the length to width ratio, and one can show that (114) satisfies $P_0(x)=P_0(1/x)$. The divergence in P_0 is a weak one and depends logarithmically on the low-energy cutoff. For macroscopic size the cutoff will be determined by the anisotropy, with the result

$$P_0\sim-\pi^{-1}\ln(N^{-1}+a^2K/2\pi^2A)$$

$$\sim\pi^{-1}\ln(2\pi^2A/a^2K)\,. \tag{115}$$

The logarithmic divergence of $\chi_\perp$, found above for dilute 2D isotropic antiferromagnets, arises from a divergence in the s-wave t matrix associated with a defect, and therefore will occur for all q. More general arguments show that the divergence is present at all concentrations above p_c, and is not an artifact of the low-concentration expansion. In Sec. VIII we shall discuss this and other sources of divergences in response coefficients which can occur away from the isolated defect limit.

To study the effects of the divergence of $\chi_\perp$ in the random 2D Heisenberg antiferromagnet we need the explicit form of $\Sigma(q,\omega)$ for $\omega\neq\omega_q$. Since this divergence comes from the s-wave scattering term [(the first term in (109)], we only analyze this term, denoted $\Sigma^{(s)}(q,\omega)$. We find it to be

$$\Sigma^{(s)}(q,\omega)=-2\omega^2+2\omega_q^2$$

$$\times\frac{[1-\delta^2P_0(\omega)][2+(1-\delta^2)P_0(\omega)]}{[1-\delta^2P_0(\omega)]^2-\delta^2P_0(\omega)^2}\,, \tag{116}$$

where $\delta=\omega/\omega_E$. For small ω^2 we have

$$P_0(\omega)\sim-(2\pi b)^{-1}\ln\frac{1}{|\omega^2|},\quad \omega^2<0 \tag{117a}$$

$$\sim-(2\pi b)^{-1}\ln\frac{1}{|\omega^2|}+(8b)^{-1}i,\quad \omega^2>0\,. \tag{118}$$

For $c \ln\omega_q \ll 1$ we can still solve (108) perturbatively and we have a damped resonance at

$$\omega^2 = \omega_q^2 [1 - (c/\pi b) \ln(1/\omega_q^2) + (c/4b) i] \ . \quad (119)$$

However, as $q \to 0$ this form yields $\omega^2 < 0$ and we must then use (118), whence

$$\omega^2 \sim -(c/\pi b)\, \omega_q^2 \ln(1/\omega_q^2) \quad (120)$$

which corresponds to an overdamped resonance. Although the dynamic response can only be evaluated exactly for $c \ll 1$, it seems likely that the qualitative behavior found for $c \ll 1$ will persist at higher c.

VII. NUMERICAL RESULTS FOR SIMPLE LATTICES

In this section we discuss computer calculations of the quantities needed to describe magnetic excitations in dilute ferromagnets and antiferromagnets with simple cubic (sc), body-centered-cubic (bcc), or simple square (sq) lattices. We present results for low and moderate concentrations of defects. The critical region close to the percolation concentration is discussed in more detail in Sec. VIII. There are a number of actual magnetic systems to which our results are applicable. A detailed review of experimental results on such model magnetic systems has been given by de Jongh and Miedema.[36] In the course of comparing our predictions with experimental measurements of the Dutch group, we found it desirable to consider the nonlinear response of these systems to a finite applied field. This extension and the resulting experimental comparisons are given in Sec. IX.

Figures 1–3 show the percolation probability $P(p)$ defined as the fraction of sites in the infinite cluster, and the exchange stiffness $A(p)$ normalized to its value for the perfect system. Both quantities are plotted as functions of p for site percolation on the sc, bcc, and sq lattices, respectively. One can use effective-medium arguments to estimate both properties by assuming that all magnetic sites are equivalent. In this way, one would estimate

$$P(p) \approx p \quad (121)$$

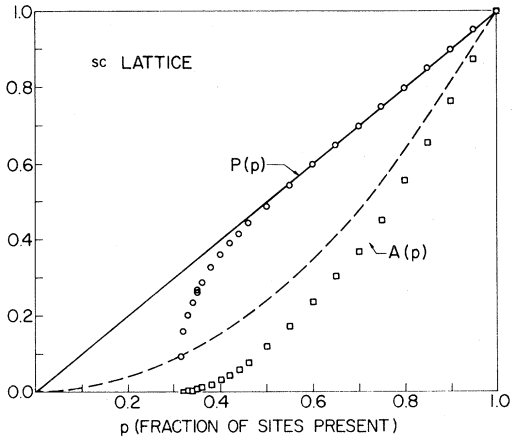

FIG. 1. Fraction of sites in the infinite cluster $P(p)$ and exchange stiffness (or conductivity) $A(p)$, normalized by $A(1)$, versus p for the sc lattice. The circles and squares represent data from Monte Carlo samples of up to $24 \times 24 \times 24$ sites [for $A(p)$] and $30 \times 30 \times 30$ sites [for $P(p)$]. The curves represent the effective medium approximations for the two quantities: (121) for $P(p)$ and (122) for $A(p)$.

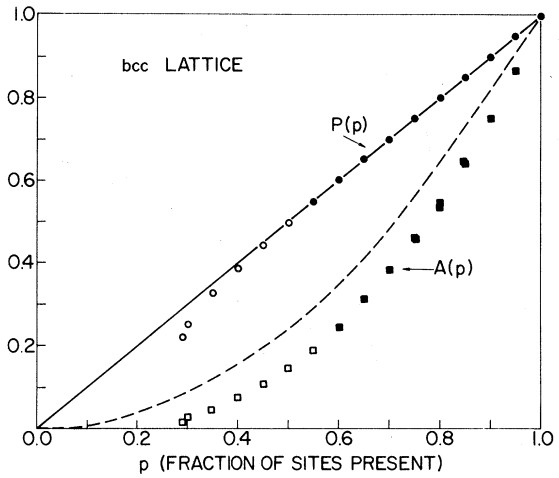

FIG. 2. Monte Carlo data and effective medium theories for $P(p)$ and $A(p)$, as in Fig. 1, but for the bcc lattice. Solid data points represent results on samples of $10 \times 10 \times 10$ unit cells, and open data points are for samples of $12 \times 12 \times 12$ cells.

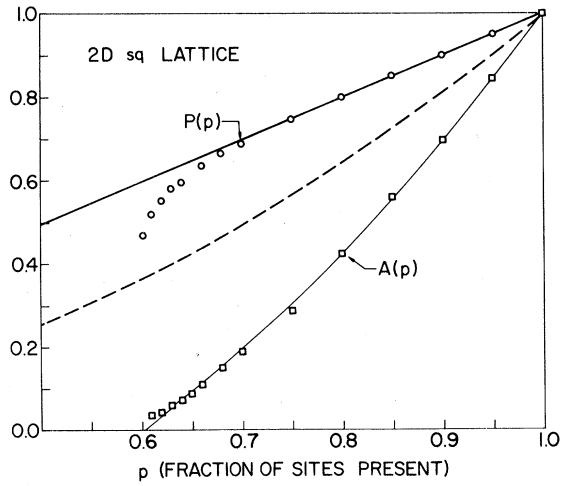

FIG. 3. Monte Carlo and effective medium theories for $P(p)$ and $A(p)$ as in Fig. 1 but for the 2D sq lattice. The data points were obtained from samples of 64×64 sites (for $p \approx 1$), and as many as 200×200 sites (for $p \gtrsim p_c$). The light solid line is the approximation (123) suggested by Watson and Leath (Ref. 41). The other curves are as in Fig. 1.

TABLE II. Limiting slopes for 3D lattices.

	fcc	bcc	sc	sq
$A^{-1}dA/dp$	2.30	2.38	2.53	3.10
$D^{-1}dD/dp$	1.30	1.38	1.53	2.10
$\chi_\perp^{-1}d\chi_\perp/dc$	···	0.98	1.02	(2.78) [a]
$C^{-1}dC/dp$	···	1.68	1.78	(2.94) [a]
$T_c^{-1}dT_c/dp$ [b]	1.36	1.32	1.37	···

[a] These quantities diverge in the limit of zero anisotropy. They were obtained by setting $\delta_A = 0.005$, as is appropriate (Ref. 7) for Rb_2MnF_4.

[b] Values of $T_c^{-1}dT_c/dp$ are given by Rushbrooke and coworkers (Refs. 37–40).

and [see I, (63)]

$$A(p) \propto p^2 . \tag{122}$$

From Figs. 1–3 we see that this effective-medium estimate of $P(p)$ is adequate above threshold except within 0.10–0.15 of p_c. The estimate $A(p) \approx p^2$, however, is quite poor. Not only does p^2 lack a threshold, but the initial slope $A^{-1}dA/dp$ is 2 for all lattices in this approximation, while the exact result (83) has the larger value, $2t_p$, which is tabulated for four lattices in Table II.[37-40] Since $2t_p - 2$ is of order z^{-1}, the error in the effective-medium estimate should be worst for the sq lattice, as Fig. 3 confirms.

In Fig. 4, we compare several approximate theories for $A(p)$ with the numerical results. One obvious way to improve the estimate $A \propto p^2$ is to substitute $P(p)$ for p, in order to obtain an estimate which vanishes as p_c. However, the threshold behavior obtained is qualitatively incorrect, as can be seen in Fig. 4.

One can use a heuristic argument due to Watson and Leath[41] to extend the exact low-concentration result in the sc and sq lattices. They argue that site percolation should be considered as a special case of bond percolation, in which pairs of bonds along a common axis, with a site in common, are removed. In bond percolation,[22,42] A is observed to decrease linearly with b, the fraction of missing bonds, until very close to threshold. Since $b = 1 - p^2 = 2c - c^2$, Watson and Leath suggest that A should be approximated by

$$A(c)/A(1) \sim 1 - 2ct_p + c^2 t_p . \tag{123}$$

This is plotted in Figs. 3 and 4, and is in excellent agreement with the calculated stiffness at concen-

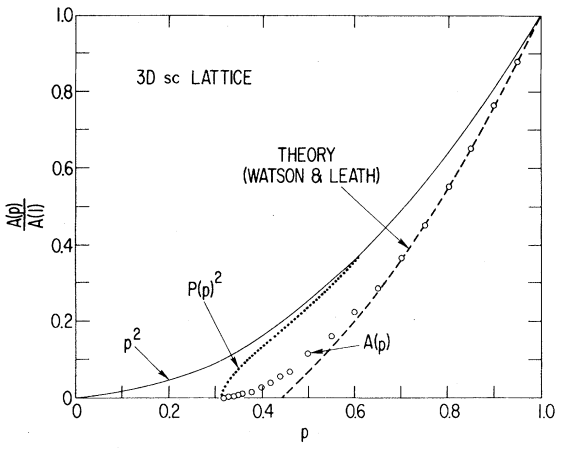

FIG. 4. Comparison of Monte Carlo data for $A(p)$ from Fig. 1 with several approximate theories, as described in the text.

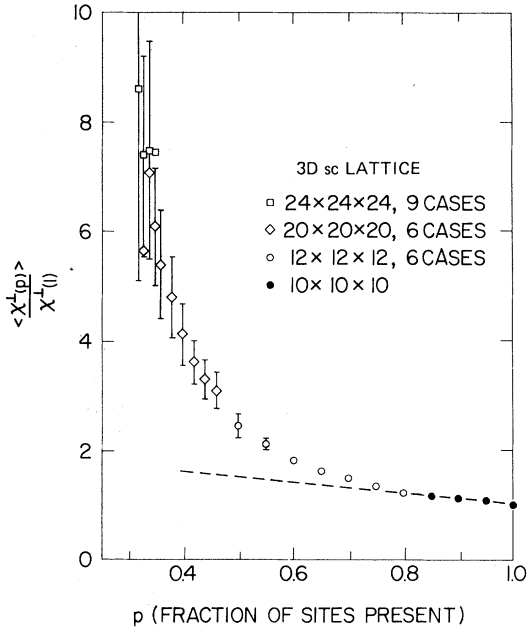

FIG. 5. Transverse antiferromagnetic susceptibility $\chi_\perp(p)$ vs p for the sc lattice. The dashed line has the exact limiting slope from low concentration theory given in Table II.

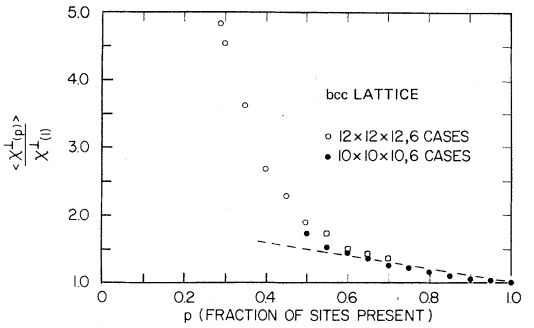

FIG. 6. $\chi_\perp(p)$ vs p as in Fig. 5, but for the bcc lattice.

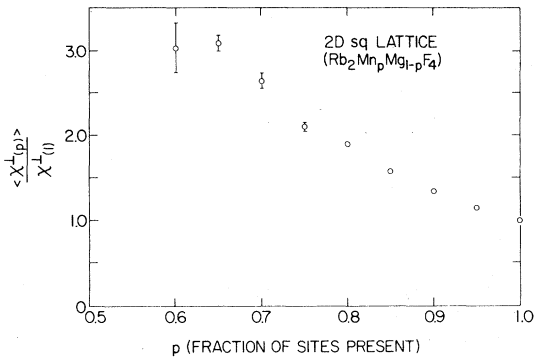

FIG. 7. $\chi_\perp(p)$ vs p for the 2D sq dilute antiferromagnet $Rb_2Mn_pMg_{1-p}F_4$, calculated using $\delta_A = 0.005$. Samples of from 40×40 to 200×200 sites were studied.

trations above 0.6 in 3D and 0.65 in 2D.

To discuss antiferromagnets we require $\chi_\perp(p)$ as well as $A(p)$. Results for $\chi_\perp(p)$, calculated for two 3D lattices in the absence of anisotropy, are presented in Figs. 5 and 6. We find that $\chi_\perp$ increases monotonically with decreasing concentration, and appears to diverge at p_c. The exact limiting slopes as $p \to 1$ can be calculated using (88), are shown as dashed lines in Figs. 5 and 6, and are given in Table II for some common lattices. The simplest mean-field-theory prediction of $\chi_\perp(p)$ can be obtained from (64) of I by setting one spin equal to zero. The result is $\chi_\perp(p) \approx \chi_\perp(1)$, implying that in this approximation the effect of looser coordination is cancelled by the decreased concentration of magnetic atoms. However, from the data in Figs. 5 and 6 and the analytic arguments given in Appendix D, it is clear that this does not happen.

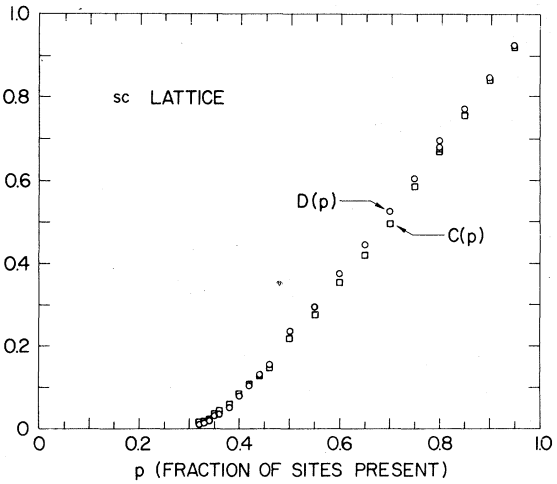

FIG. 8. Spin-wave dispersion coefficients, $D(p)$ and $C(p)$ (normalized to their values at $p = 1$) for the sc lattice as given by (13b) and (20) and the data of Figs. 1 and 5.

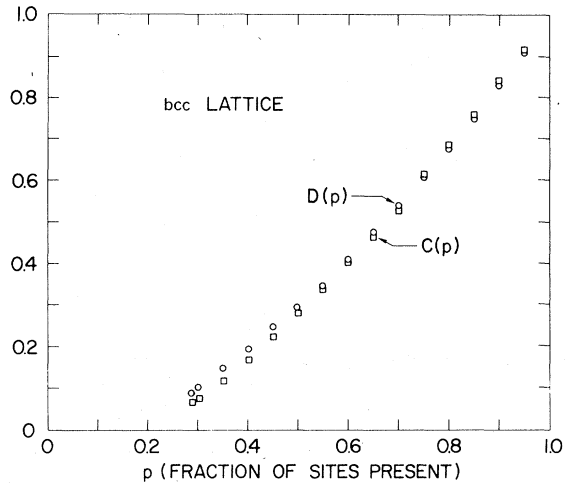

FIG. 9. $D(p)$ and $C(p)$ vs p as in Fig. 8 but for the bcc lattice, using the data of Figs. 2 and 6.

Thus the actual response, increasing with increasing defect concentration, must be nonuniform. The exact limiting slopes of the physical quantities A, $\chi_\perp$, C, and D, calculated by the methods of Section V, are given in Table II for some common lattices.

For 2D systems, $\chi_\perp$ is only meaningful in the presence of an anisotropy field H_A which limits $\chi_\perp$ to be $< g^2\mu_B^2 S_{av}/H_A$. Therefore, to study a 2D case, we used the parameters appropriate to $Rb_2Mn_pMg_{1-p}F_4$, where Mg is nonmagnetic. The exchange interaction $J_{MnMn} = 0.328$ meV as in I, while $\Delta_{Mn}(p) = 0.03p$ meV was taken to be dependent upon concentration, since the Mn anisotropy is almost purely dipolar,[43] and thus proportional to the sublattice magnetization. Figure 7 shows $\chi_\perp(p)$ for the sq lattice with this choice of parameters. For this 2D case with anisotropy, $\chi_\perp$ does not increase as dramatically near p_c, nor is the scatter in the data as great as in the isotropic 3D cases shown in Figs. 5 and 6.

The spin-wave dispersion coefficients C and D, as determined by (20) and (13b), respectively, are plotted in Figs. 8 (sc), 9(bcc), and 10(sq). From the figures it is apparent that D and C scale with concentration in very similar ways. However, the limiting slopes given in Table II are different and the behavior of the two quantities at threshold, discussed in Sec. VIII, also differs, so they are only approximately equal, and may show quite different dependences in systems with other lattice structures or other types of disorder.

All of the data in Figs. 1–10 were obtained by exact solution of the equations describing the linear response of a finite sample to various external fields. The factorization procedure used to invert these equations has been described in Ap-

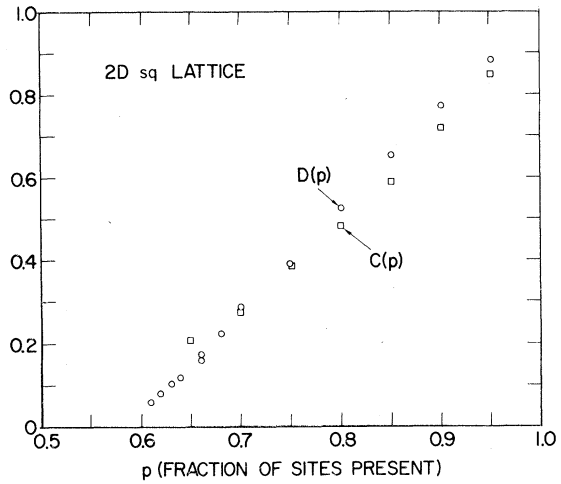

FIG. 10. $D(p)$ and $C(p)$ vs p as in Fig. 8 but for the 2D sq lattice using the data of Figs. 3 and 8. $C(p)$ represents the linear dispersion seen above the anisotropy gap in $Rb_2Mn_pMg_{1-p}F_4$.

pendix A of I. The dilute systems studied here differ from the two-component alloy considered in I in that one cannot take advantage of the symmetry of the lattice to reduce the effort required to factorize the system of equations. However, the standard (modified Markowitz[44]) sparse matrix methods are quite effective on the dilute systems. It proved possible to solve 2D lattices as large as 200×200 sites, and 3D cases as large as $24\times 24\times 24$ at concentrations close to the respective percolation thresholds. For cases in which $p\approx 1$, lattices with 10^3 and 12^3 sites were used in 3D and 64^2 to 80^2 sites were studied in 2D. Samples of several sizes were solved at each concentration. The results from larger samples generally fell within one standard deviation of the results of smaller samples, so we did not attempt to extrapolate the results to infinite sample size.

One can check the validity of finite sample simulations for $p\approx 1$ by calculating exactly the effect of a single defect in a sample of a given size, and comparing this with the low-concentration results for infinite systems described in the preceding section. We have calculated P_0 and t_p for finite samples, replacing Fourier integrals by the appropriate sums. Sample size has relatively little effect on t_p. For an sc sample of 8^3 sites, t_p is only 0.3% less than for an infinite lattice, and for an sq lattice of only 16^2 sites, t_p was within 0.6% of its limiting value. We conclude that $A(p)$ can be very accurately simulated with samples of the size employed in this study.

P_0, and hence the simulation of $\chi_\perp(p)$, is much more sensitive to size effects. The energy denominator involved, $1-\gamma_q$, is singular, causing the lattice sum to converge very slowly to the Fourier integral. For a 10^3-site sc sample, we anticipate that $\chi_\perp^{-1}\,d\chi_\perp/dc$ will be roughly 10% below the exact result of Table II. The data plotted in Fig. 5 for $p\gtrsim 0.8$ show this discrepancy. In the presence of anisotropy, this size dependence is reduced. For a typical value of $\delta_A\approx 0.005$ (appropriate[7] to Rb_2MnF_4) the error in P_0 for a 10^3-site sc sample is only 3%. In 2D, of course, P_0 for an infinite sample exists only in the presence of anisotropy, so it should be more size dependent in 2D than in 3D. However, for $\delta_A=0.005$ we find that P_0 for a 32×32 sample is only 7% below its limiting value, while for a 64×64 sample (a numerically tractable size), the error was less than 2%. It therefore does not appear that finite sample size is a serious limitation on calculations of static elastic constants for realistic systems.

Although all of the physical quantities discussed in this paper have been calculated at $T=0$, it is natural to ask whether any information about the concentration dependence of the ordering temperature T_c has been obtained. The initial slope of $T_c(p)$ at $p=1$ has been established for the Heisenberg ferromagnet on several 3D lattices by Rushbrooke and co-workers,[37-40] in a series of papers analyzing high-temperature series expansions. Their results are compared, in Table II, with the limiting slopes of the zero-temperature quantities A and D, which were calculated exactly in Sec. V.

In all cases the slope of A is much greater than that of T_c, while for the fcc and bcc lattices the slope of D is roughly equal to $T_c^{-1}\,dT_c/dp$. However, this agreement is most likely fortuitous. We shall see below that the slope of D bears no relationship to $T_c^{-1}\,dT_c/dp$ in garnets, while it has been proposed in the garnet literature[45] that $A(p)/A(1)$ is equal to $T_c(p)/T_c(1)$. Furthermore, the slopes of T_c tabulated in Table II apply to Heisenberg ferromagnets with $S=\frac{1}{2}$ or 1. In the fcc case, for which the series are best established, $T_c^{-1}\,dT_c/dp$ has also been obtained for the classical ($S=\infty$) Heisenberg model, and is only 1.15. Since our calculated slopes are independent of spin, and represent a classical limit, it therefore seems unlikely that any reliable empirical relationship between D and T_c exists for these simple model systems.

VIII. PERCOLATION THRESHOLD AND OTHER SINGULARITIES

It is interesting to consider the behavior of the various elastic constants in the limit $p\to p_c$. Quantities such as the fraction of sites in the infinite cluster $P(p)$, the mean-square cluster size $S(p)$, the "cluster specific heat" $C(p)$, and the pair connectedness correlation length $\xi(p)$, have recently

TABLE III. Values of geometric and response function exponents. (Parentheses indicate values obtained by scaling relations.)

	2D	3D	Mean field
β	0.14 ± 0.005 [a]	0.39 ± 0.005 [b]	1 [c]
γ	2.3 ± 0.1 [d]	1.8 ± 0.05 [b]	1 [c]
α	-0.65 ± 0.1 [e]	(-0.58) [f]	-1 [f]
ν	(1.29) [f], 1.4 [g]	(0.86) [f], 0.95 [h]	$\frac{1}{2}$ [i]
σ	1.1 ± 0.1 [j]	1.6 ± 0.1 [j]	3 [k]
τ	...	0.5 ± 0.2 [j]	0 [j]
ζ	(1.1) [l]	(0.7) [l]	1 [m]

[a] See Refs. 47, 49, and 50.
[b] See Ref. 49.
[c] See Ref. 51.
[d] See Refs. 47–50.
[e] See Refs. 47 and 49.
[f] Using scaling relations $\alpha = 2 - 2\beta - \gamma$, or $d_\nu = 2\beta + \gamma$. See Ref. 46.
[g] See Refs. 47 and 52.
[h] See Refs. 52.
[i] See Ref. 53.
[j] This work.
[k] See Ref. 54.
[l] Obtained using (128).
[m] See Ref. 55.

been shown[46] to be analogous to thermodynamic properties of those magnetic systems whose critical phenomena are now understood through renormalization-group arguments.[47] In the limit $p \to p_c$ we define the various exponents of interest by

$$P(p) \sim |p - p_c|^{\beta} \quad (p \to p_c^+), \tag{124a}$$

$$S(p) \sim |p - p_c|^{-\gamma}, \tag{124b}$$

$$C(p) \sim |p - p_c|^{-\alpha}, \tag{124c}$$

$$\xi(p) \sim |p - p_c|^{-\nu}. \tag{124d}$$

In addition to these purely geometrical properties, we consider the exponents describing the magnetic elastic responses in a dilute lattice for $p \to p_c^+$:

$$A(p) \sim |p - p_c|^{\sigma}, \tag{125a}$$

$$\chi_\perp(p) \sim |p - p_c|^{-\tau}, \tag{125b}$$

where $\chi_\perp(p)$ applies to a dilute antiferromagnet.

In Table III[48-55] we list our numerical results for σ and τ. Because of the enormous scatter in $\chi_\perp(p)$ for p close to p_c, we could only estimate τ to 30% accuracy in the sc case, and did not attempt to determine it for the bcc case. We also list in Table III the most recent values of the geometrical exponents defined in (124) for two- and three-dimensional lattices, as well as the mean-field values. As is well known, critical exponents assume their mean-field values when the spatial dimensionality d is larger than some critical value d_c. For $d < d_c$ the scaling relations hold and the exponents vary continuously as a function of d. For the geometrical exponents defined in (124), Toulouse[53] has pointed out that the mean-field values of the exponents are those of the Cayley tree. From these exactly known[51,53] exponents he infers that $d_c = 6$ for the percolation problem. Renormalization-group expansions of the percolation exponents in powers of $\epsilon \equiv d_c - d$ have been developed.[47] This was possible because the percolation problem may be expressed in terms of a field theory involving local variables.[46]

Much less is known about the exponents σ and τ. de Gennes[54] has recently proposed that $\sigma = 3$ in mean-field theory, using an argument which we extend below to obtain the mean-field result $\tau = 0$. de Gennes argues that for $d < d_c$

$$A \sim L^{-1} \xi^{2-d}, \tag{126}$$

where L is a characteristic path length between "irreducible nodes"[56] of the random network. Accordingly, we are led to introduce another exponent

$$L \sim |p - p_c|^{-\zeta} \quad (p \to p_c^+). \tag{127}$$

Mean-field theory,[55] i.e., the Cayley tree, yields $\zeta = 1$. de Gennes postulates that this holds for all d. As we shall see, the numerical evidence does not support this conjecture. One sees that (126) gives

$$\sigma = \zeta + (d - 2)\nu, \tag{128}$$

and insertion of mean-field values into this relation shows that $d_c = 6$, as expected. In Table III, we give the values of ζ obtained using (128). The suggested relation $\zeta \equiv 1$ appears to lie outside the error bars. Substituting (124) and (125) into the definitions (13b) and (20) of D and C we find a threshold exponent of $\sigma - \beta$ for D and $\frac{1}{2}(\sigma + \tau)$ for C. In 3D these are ≈ 1.2 and 0.9, respectively. Thus the differences between $D(p)/D(1)$ and $C(p)/C(1)$, discussed in the preceding section, persist in the critical region near p_c.

We may obtain some information about $\chi_\perp$ by a simple estimate of the effects of fluctuations as follows. We consider a system where $\langle S_i^z \rangle$ is a random variable. This may be due to either dilution, in which case $\langle S_i^z \rangle$ assumes the values S_i or 0, or to fluctuation in the sign of J_{ij} so that $\langle S_i^z / S \rangle$ assumes the values ± 1. Whereas in the pure antiferromagnet the total spin $\sum_i \langle S_i^z \rangle$ summed over a unit cell vanishes, this is no longer true in the presence of random variations in $\langle S_i^z \rangle$. We now make a simple estimate of the effects of this type of disorder on $\chi_\perp$. To do this we subdivide the initial volume V consisting of N sites into m volume elements v_i, each containing l^d sites, where d is the dimensionality. There are thus $N\, l^{-d}$ such volume elements. On the average, the mean-square unbalanced spin in v_i is $S^2(v_i) \sim l^d$. Now fix the spins on the boundary of each v_i to be parallel to z, so that the exchange interactions between different v_i's vanish. We now calculate the effect of

an applied field, $h(\vec{r})\hat{x}$, on v_i. Consider the energy of v_i in the presence of a spin-density wave (SDW)

$$\vec{S}(\vec{r}) = S_i^z[(1-\theta_r/2)\hat{z} + \theta_r\hat{x}], \tag{129}$$

with

$$\theta_r = a_q \sin qx \sin qy \sin qz, \tag{130}$$

where $q = 2\pi/l$ is chosen so that θ_r vanishes on the boundary of v_i. Note that this SDW rotates both sublattices so that locally they remain parallel. Then the exchange energy is of order $l^d a_q^2 q^2$ and the total energy of v_i is

$$E(v_i) = C_1 l^d a_q^2 q^2 - C_2 S(v_i) a_q h_0, \tag{131}$$

where C_1 and C_2 are constants. The second term in (131) is the Zeeman energy of the unbalanced spin. Minimizing $E(v_i)$ with respect to a_q, we determine that

$$a_q \propto S(v_i) l^{2-d} h_0, \tag{132}$$

so that the transverse moment per site, $m_\perp$, i.e., $h_0 \chi_\perp$, is of order

$$m_\perp \sim S(v_i)^2 l^{2-2d}. \tag{133}$$

Since $S(v_i)^2 \propto l^d$, this estimate gives

$$m_\perp \geq l^{2-d}. \tag{134}$$

We obtain an inequality in (134) because the constrained response we have estimated is certainly less than the unconstrained response. The result (134) indicates that in the presence of this type of disorder $d=2$ is the critical dimensionality below which the antiferromagnetic state is unstable with respect to application of a small transverse field.[57]

Clearly this construction is too crude to show in what way $m_\perp$ diverges for $d=2$. But that was to be expected in view of the single-vacancy result which indicated that $m_\perp \propto \ln N$, or in this case $m_\perp \propto \ln l$. However, since $\tau = 2-d = 0$ for $d=2$ is the correct exponent for a logarithmic divergence, we are encouraged to refine the construction. The details of this more complete argument, which gives $\chi_\perp \sim \ln N$, are contained in Appendix C. Note that the form of divergence in the limit $N \to \infty$, which we find in one and two dimensions agrees with the exact results for special models given in Sec. V, as well as with the low-concentration results given in Sec. VI.

For $d>2$, a refinement of the above argument may be used to obtain a bound on the exponent, τ, of $\chi_\perp$. For this purpose we write (133) in an alternative form as

$$\chi_\perp \geq S(v_i)^2 / l^{2d} A q^2. \tag{135}$$

We write the total spin as

$$S(v_i)^2 = \left[\sum_i p_i \langle S_i^z \rangle\right]^2 \tag{136}$$

and estimate it as proportional to the number of occupied sites in the infinite cluster, i.e., of order $l^d |p-p_c|^\beta$, using (124a). If we also substitute (125a) and $q \sim l^{-1}$, we obtain

$$\chi_\perp \geq |p-p_c|^{\beta-\sigma} l^{2-d}. \tag{137}$$

For a fixed l we cannot let $p \to p_c$, because the asymptotic forms (124) and (125) are only valid if $l > \xi$. The best possible valid estimate is therefore found by setting $l = \xi \sim |p-p_c|^{-\nu}$. Then, if we also assume Eq. (125b), we find

$$\tau \geq \sigma - \beta + (2-d)\nu. \tag{138}$$

It would not be surprising if this inequality was actually an equality, as occurs for other critical phenomena,[58] at least for $d>2$. From Table III we see that (138) is satisfied for three dimensions, and may indeed hold as an equality.

We may construct an estimate for $\chi_\perp$ analogous to (126) by using de Gennes's arguments. Sufficiently close to p_c one may view the random network as consisting of "nodes" connected by strands with characteristic length L bonds. The nodes are separated by a characteristic distance of approximately ξ. We now consider constructing a constrained response as was done in Eqs. (129)ff. For this purpose we assign an unbalanced spin to each node by associating a volume Ω with each node within which all spins are required to tip uniformly in response to the applied transverse field. We take $\Omega \sim \xi^d$. According to the construction shown in Fig. 11 we may still assume that the strand connecting adjacent volumes is of order L in length. Along the strands the spin direction can

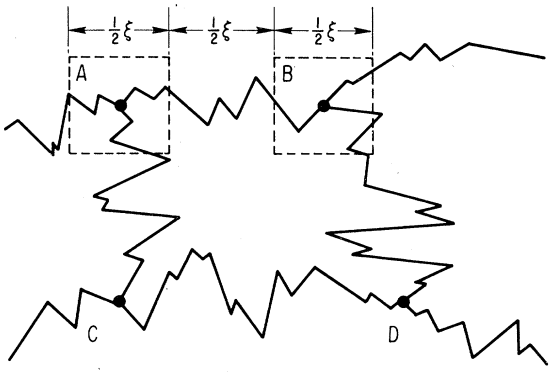

FIG. 11. Schematic representation of a dilute network near the percolation threshold. The arc length along paths separating nodes A, B, C, and D (each connected to the "point" at infinity) is of order L and the distance (as the crow flies) between adjacent nodes is of order ξ. We associate a volume of linear dimension $\frac{1}{2}\xi$ with each node. The path connecting different volume elements is then of order $\frac{1}{2}L$.

vary slowly, so that the strand can be described by a single interaction of order J/L. (This is equivalent to saying that the conductance of a strand is of order σ_0/L, where σ_0 is the conductance of a single bond.) As argued following (136), the unbalanced spin in Ω is of order $\xi^d P(p)$. Thus the susceptibility per site is of order

$$\chi_\perp \sim \xi^d P(p)(J/L)^{-1}/\xi^d \sim LP(p)\,. \tag{139}$$

Thus we have

$$\tau = \zeta - \beta\,, \tag{140}$$

and in particular the mean-field results $\zeta = 1, \beta = 1$ imply that the mean-field value of τ is 0.

We note that (128) and (140) imply that (138) holds as an inequality. Substituting the mean-field values of σ and τ into (138), we conclude that $d_c = 6$ for $\chi_\perp$ as well as for A, as one would expect since they both depend upon L. To date, no field theory or renormalization-group treatment for either $\chi_\perp$ or A has been established to extend this picture below six dimensions. [Since the completion of this work, however, approximate renormalization groups have been constructed for $A(p \to p_c)$ on specific 2D and 3D lattices,[79] with results confirming (125a) and in good agreement with Table III.]

It should also be noted that there is a difference in interpretation between the work of de Gennes[54] and Stinchcombe.[55] de Gennes gives $\sigma = 3$ as the mean-field limit, while Stinchcombe obtains $\sigma = 2$. This difference can be attributed to the factor $L \sim (p - p_c)^{-1}$ which appears in (126). An estimate of $\chi_\perp$ analogous to Stinchcombe's would give (139) without the factor L, so that $\tau = -1$. In any event, (138) would hold since it involves only $\tau - \sigma$, which is independent of ζ, the exponent associated with L.

IX. NONLINEAR SUSCEPTIBILITY

Breed and co-workers have carried out detailed measurements[1-3] of the magnetic properties of several antiferromagnetic alloys which closely approach the idealized models treated in the preceding sections. They have studied, in particular, $KMn_pMg_{1-p}F_3$ and $K_2Mn_pMg_{1-p}F_4$. The former is found to be a very isotropic Heisenberg antiferromagnet, with $\delta_A \equiv H_A/H_E < 10^{-5}$, and $J = -0.345$ meV (4.0 K),[2] independent of concentration. The magnetic atoms occupy the sites of a simple cubic lattice, and nonmagnetic Mg^{2+} ions apparently substitute randomly for the $Mn^{2+}(S = \frac{5}{2})$ ions. K_2MnF_4 is accurately described as a 2D square antiferromagnet, the Mn^{2+} ions confined to well-separated planes in the crystal structure. Interactions between planes give rise to an anisotropy $\delta_A \approx 0.004$.[4] There is evidence from the Curie-Weiss plots of $\chi(T)$ at high temperatures that $|J|$ increases with dilution in $K_2Mn_pMg_{1-p}F_4$. Breed *et al.* find J/k

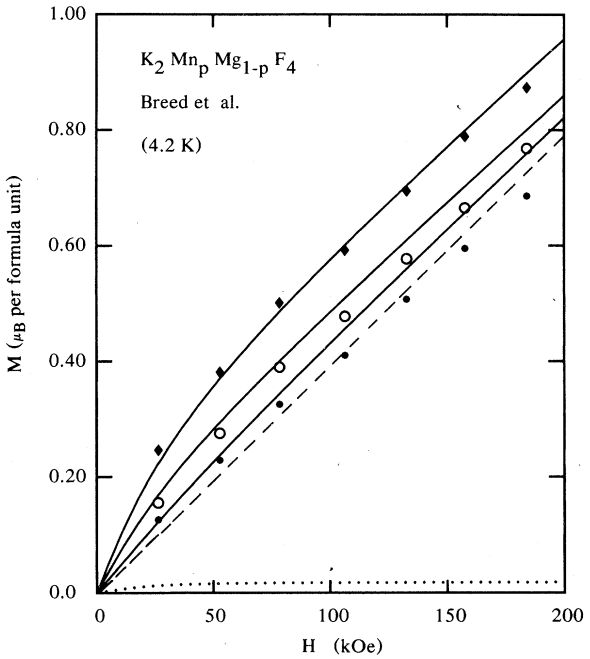

FIG. 12. Magnetic moment per site M, at low temperature as a function of transverse field for dilute $K_2Mn_pMg_{1-p}F_4$ alloys at several concentrations (data from (Ref. 2). The diamonds are for $p = 0.74$, the circles for $p = 0.84$, and the dots for $p = 0.93$. The solid lines give the corresponding magnetization as calculated numerically, as described in the text, using samples of 80×80 sites ($p = 0.74$), 60×60 sites ($p = 0.84$), and 44×44 sites ($p = 0.93$). The dashed line indicates the magnetization expected for pure K_2MnF_4. The dotted curve shows the contribution of the isolated clusters included in the calculated magnetization for $p = 0.74$.

$\approx -4.2[1 + 0.43(1 - p)]$, and interpret the increase as a result of the discrease in over-all lattice constant upon doping with the smaller Mg ions. The large magnitude of the Mn spin makes the classical treatment of this paper an appropriate first approximation to the properties of these systems.

Calculations[10,17,59] of high-frequency excitations in randomly substituted Heisenberg magnets, giving detailed agreement with results of neutron scattering,[6,7] have appeared elsewhere. In this section we compare the static susceptibility calculated by our methods with Breed's measurements, to check our predictions of the increase of $\chi_\perp$ on dilution and of the divergence at p_c. The experimental data does support our picture of the importance in $\chi_\perp$ of ferrimagnetic fluctuations, but in a way which was not anticipated.

The most obvious feature of the experimental data at low temperatures, plotted in Figs. 12 and 13, is the nonlinear field dependence of the magnetization. In both 2D and 3D, the low-field susceptibility increases with decreasing concentration, while the susceptibility at high fields re-

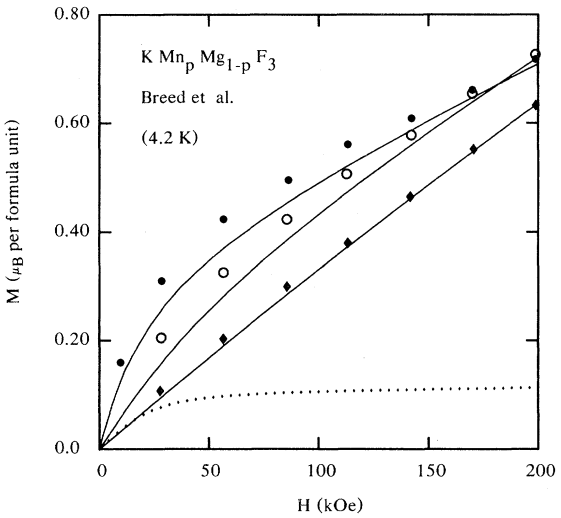

FIG. 13. Magnetization as a function of transverse field at low temperature in $KMn_pMg_{1-p}F_3$ (data from Ref. 2). The diamonds represent $p=0.82$, the circles are $p=0.58$ and the dots are for $p=0.39$. The solid lines give the calculated magnetizations for these concentrations, including the effects of isolated clusters. Samples sizes used are $24\times24\times24$ ($p=0.39$), $14\times14\times14$ ($p=0.58$), and $8\times8\times8$ ($p=0.82$). The dotted curve gives contribution to the magnetization for $p=0.39$ obtained by enumeration and exact solution of clusters of four or fewer sites.

mains constant or decreases. The curvature of the plots of M vs H increases with decreasing concentration, and is slightly greater in the highly isotropic 3D alloys shown in Fig. 13 than in the data from the more anisotropic 2D alloys (Fig. 12).

Isolated finite clusters of spins play a minor role in the nonlinear field dependence seen in Figs. 12 and 13. To begin with, they are relatively rare. For the 2D case with $p=0.74$, numerical study shows that only 0.65% of the magnetic sites lie in isolated clusters. For the two higher concentrations, less than one magnetic site in 10^4 is isolated. For the 3D case with $p=0.39$, $p-P(p)$ is found to be ≈0.047; for $p=0.58$ it is ≈0.007, and for $p=0.82$ it is negligible.

It is not difficult to calculate exactly, for clusters of a few spins, the moment induced per site in fields up to 200 kOe at 4.2 K. We have done this for clusters containing one to three adjacent Mn atoms, and also for clusters with three spins on one sublattice adjacent to one on the other sublattice. We treat these small clusters since they are the most common, and larger clusters do not have as great a net moment per site at low fields. Above ≈ 50 kOe, those clusters with a net moment in zero field are oriented parallel to $h_{\rm ext}$, while fields of order 200 kOe begin to overcome the exchange fields, and draw moments of roughly $\frac{1}{2}S$ per site even from isolated pairs of spins, which have no zero-field moment. For each of the concentrations shown in Figs. 12 and 13, we summed the contributions from these small clusters with appropriate weights. The result is shown as a dotted line for the case of lowest concentration in each figure, and proves to be negligible for the higher-concentration cases in both figures. In all cases, adding this cluster moment to the linear response characteristic of a uniform material fails to account for the observed curvature in M versus $h_{\rm ext}$.

The ferrimagnetic fluctuations discussed in the previous sections do provide a mechanism for the nonlinear response, and conversely this type of high-field measurement appears to provide a method for the direct observation of such fluctuations. In the construction of a lower bound to $\chi_\perp$, (129)–(134), it was found that large contributions to $m_\perp$ came from regions in which the net spin differed from zero by one or more standard deviations. In the presence of a finite external field, the spins in such regions may deviate through angles large enough to cause the small angle approximation made in calculating $\chi_\perp$ to break down. Thus we argue that the low-field limit of $\partial M/\partial H$ in Figs. 12 and 13 should be identified with $\chi_\perp$ as calculated in Secs. VI and VII, and that the nonlinearity arises from the gradual saturation of the response of the ferrimagnetic fluctuations.

This can be checked quantitatively by examining the microscopic details of a computer simulation similar to those of Sec. VI. First we give an expression for the microscopic energy in the presence of a uniform field $\vec{h}=h_{\rm ext}\hat{x}$ in a form which makes the angular dependence explicit:

$$e_{\rm tot}=-2|J|\sum_{i,j}p_ip_jS_iS_j\cos(\theta_i+\theta_j)-\sum_i\Delta_ip_iS_i\cos\theta_i-g\mu_B\sum_i p_iS_ih_{\rm ext}\sin\theta_i\,, \tag{141}$$

where θ_i is the angle through which $\vec{S}_i$ relaxes in the x-z plane as in (50). The equilibrium conditions (44) become

$$2|J|\sum_j p_jS_iS_j\sin(\theta_i+\theta_j)+\Delta_iS_i\sin\theta_i=g\mu_BS_ih_{\rm ext}\cos\theta_i\,. \tag{142}$$

In order to derive an efficient iteration procedure to solve (142), we write it as

$$Q_i = \sum_j 2|J|p_j S_i S_j (u_i v_j + v_i u_j) + \Delta_i S_i u_i - g\mu_B h_{\text{ext}} S_i v_i = 0, \tag{143}$$

where u_i, v_i denote $\sin\theta_i, \cos\theta_i$. If an approximate solution $\{u_j\}$ is changed by $\{\delta u_j\}$, the resulting change in Q_i is

$$\delta Q_i = \sum_j K_{ij} v_j^{-1} \delta u_j , \tag{144}$$

where

$$K_{ij} = \delta_{ij}\left(\sum_k 2|J|p_k S_i S_k (v_i v_k - u_i u_k) + \Delta_i S_i v_i + g\mu_B h_{\text{ext}} S_i u_i\right) + 2|J|p_j S_i S_j (v_i v_j - u_i u_j). \tag{145}$$

At each iteration, assume that the $\{u_j\}$ are a reasonable first guess to the solution of (143). For example, the $\{u_j\}$ might be the correct result for a slightly smaller value of h_{ext}. Then a good choice of $\{\delta u_j\}$, such that $Q_i(\{u_j + \delta u_j\})$ vanishes to first order in all δu_j, is given by

$$\delta u_i = -\sum_j v_i (\underline{K}^{-1})_{ij} Q_j(\{u_k\}) . \tag{146}$$

One precaution is necessary. To avoid making any $|u_i| > 1$, large increments must be compressed. The incrementing formula

$$\begin{aligned} u_i^{(n+1)} &= u_i^{(n)} + \delta u_i \{1 + [\delta u_i/(1-u_i)]^2\}^{-1/2}, \quad \delta u_i > 0 \\ &= u_i^{(n)} + \delta u_i \{1 + [|\delta u_i|/(1+u_i)]^2\}^{-1/2}, \quad \delta u_i < 0 \end{aligned} \tag{147}$$

has the property that $Q_i^{(n+1)}$ remains of order δu^2 and $|u_i| < 1$. Using (146) and (147), it was possible to obtain solutions to the nonlinear equations (142), with a maximum error of 10^{-5} in any of the u_i in two or three iterations, whenever $h_{\text{ext}} \leq 0.1 H_E$, starting with all angles zero, and for larger values of h_{ext} by starting with a solution for a field roughly half as great.

The magnetization as a function of field was calculated by this procedure for each of the experimental concentrations, using the parameters given in Ref. 2. The contribution of isolated clusters was added where significant, and the results are given by the solid lines in Figs. 12 and 13. Theory and experiment agree to well within the uncertainty in Breed's determination of J for the cases $p = 0.74$ and $p = 0.84$ in Fig. 12. We have no explanation for the discrepancy at high fields between the theory and the experimental points for $p = 0.93$. Since the data points lie below the response expected for pure K_2MnF_4 (the dashed line), the cause must lie outside of the mechanisms discussed in this section.

The data on the 3D system $KMn_pMg_{1-p}F_3$ (Fig. 13) also agree well with the calculations. Agreement could be improved by performing the numerical calculations on larger samples, since this would improve the treatment of fluctuations of large spatial extent, and thus enhance the magnetization at low fields without increasing it greatly at higher fields. One might also extend the calculations of finite-cluster contributions for the case $p = 0.39$. Since a rough calculation suggests that the dotted line in Fig. 13 represents at least $\frac{2}{3}$ of the isolated-cluster moment, and exact solution of much larger clusters is prohibitively difficult, we did not attempt this. It seems valid to conclude from Figs. 12 and 13 that ferrimagnetic fluctuations do account for the unusual observed magnetization, and that this sort of nonlinear susceptibility may be considered indicative of an inhomogeneous response on the atomic scale.

Figures 14–16 provide a microscopic examination of the fluctuations. In Fig. 14 we show the distribution of values of $\sin\theta_i$ observed in the 3D simulations at three concentrations, in each case using $h_{\text{ext}} = 30$ kOe. The distributions extend to negative deviations in all cases. The distribution broadens as the concentration is decreased, and the rate at which it broadens exceeds the rate at which the average spin deviation increases. In contrast to Fig. 14, the distribution of $\cos(\theta_i - \theta_j)$, which determines the exchange energy associated with each bond, is found to remain sharp until much higher fields. Thus the two sublattice moments remain nearly opposite everywhere, but the moment in regions where one sublattice dominates can swing into the field by appreciable angles. The snapshots of equilibrium spin orientations shown in Figs. 15 and 16 confirm this picture.

Figure 15 shows a single layer of a 3D sample with p in the vicinity of p_c. In the smallest fields applied [Fig. 15(a)], the local orientation of the sublattice magnetzation swings through angles of up to 45°. [The field applied in Fig. 15(a) is roughly 2800 Oe, if we use parameters appropriate to $KMnF_3$.] Doubling the field [Fig. 15(b)] produces only slight increases in this over-all relaxation. In both Figs. 15(a) and 15(b), neighboring spins remain very nearly antiparallel throughout. Another fourfold increase in h_{ext} [Fig. 15(c)] be-

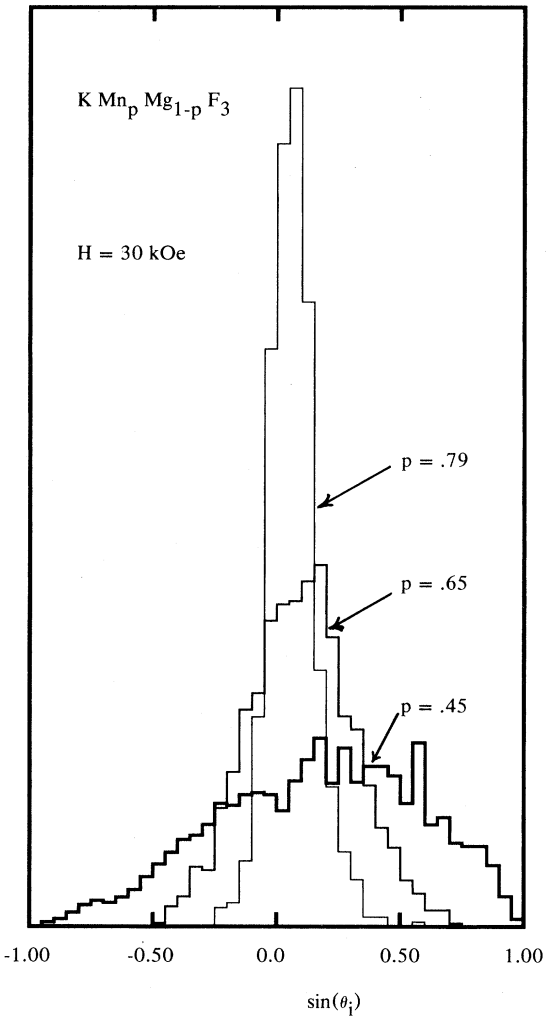

FIG. 14. Distribution of transverse spin deviations ($\sin\theta_i$ is plotted) in an applied field of 30 kOe for $KMn_pMg_{1-p}F_3$ for three dilutions. The calculations are based on (142) and were carried out for samples similar to those used in Fig. 13.

gins to draw the two sublattices out of alignment locally.

The local relaxation decreases rapidly with increasing concentration. Figure 16(a) shows the effect of applying the same field to a $p=0.55$ sample as was applied in Fig. 15(a) to a more dilute sample. Deviations from the easy axis are less than 10° everywhere. Applying a field $h_{\rm ext}=0.067H_E$, as shown in Fig. 16(b), produces spin deviations comparable to those shown in Figs. 15(a) and 15(b). In the terms of the preceding section [e.g., (139)], this suggests that $L(0.40)$ is from four to eight times as great as $L(0.55)$. Finally, application of a large field to the sample [Fig. 16(c)] produces large local deviations between the two sublattices. [Using $KMnF_3$ parameters, $h_{\rm ext}$ in Fig. 16(c) is of order 120 kOe.]

The microscopic phenomena seen in Figs. 14–16 should be experimentally accessible. Experiments such as nuclear magnetic resonance or Mössbauer effect, which probe the induced hyperfine field at a nonmagnetic impurity site, will measure the net moment of the neighboring magnetic ions. In a sufficiently dilute antiferromagnet, these ions may relax almost independently, even though they may be separated by only a few lattice sites, as occurs at the circled sites in Fig. 15. Thus the ferrimagnetic fluctuations will cause a field-dependent broadening of the observed hyperfine fields.

A more direct and easily interpreted measurement is neutron diffraction to measure the static susceptibility at finite wave vector. This is given by

$$\chi^{+-}(\vec{q},0)\propto\int\langle\vec{m}_\perp(\vec{r})\cdot\vec{m}_\perp(\vec{r}')\rangle \times\exp[i\vec{q}\cdot(\vec{r}-\vec{r}')]\,d\vec{r}\,d\vec{r}', \qquad (148)$$

where $\vec{m}_\perp(\vec{r})$ denotes the component of $\vec{m}(\vec{r})$ perpendicular to $\vec{q}$. We now consider an experiment

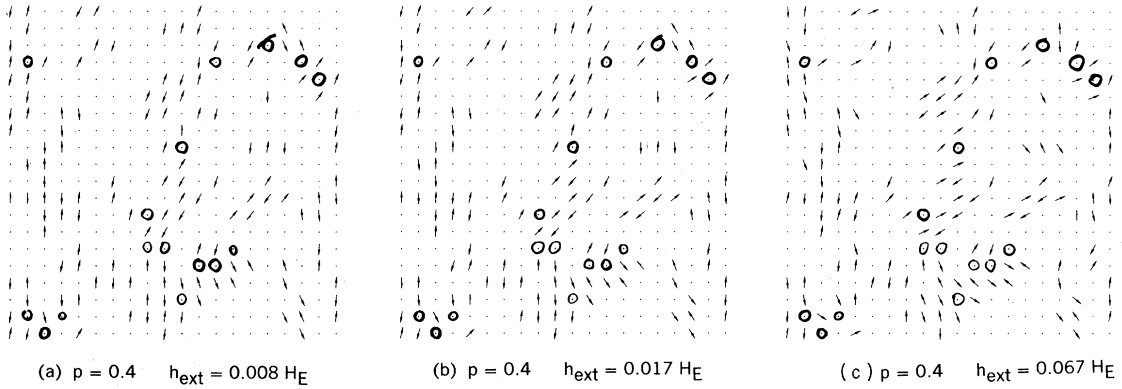

FIG. 15. Equilibrium orientations of the spins in one layer of a randomly diluted 3D ($20\times20\times20$ site) antiferromagnet with a concentration of 0.40 and transverse applied fields (a) $h_{\rm ext}/H_E=0.008$, (b) $h_{\rm ext}/H_E=0.017$, and (c) $h_{\rm ext}/H_E=0.067$. Some nonmagnetic sites at which the hyperfine field broadening described in the text would be observed are circled.

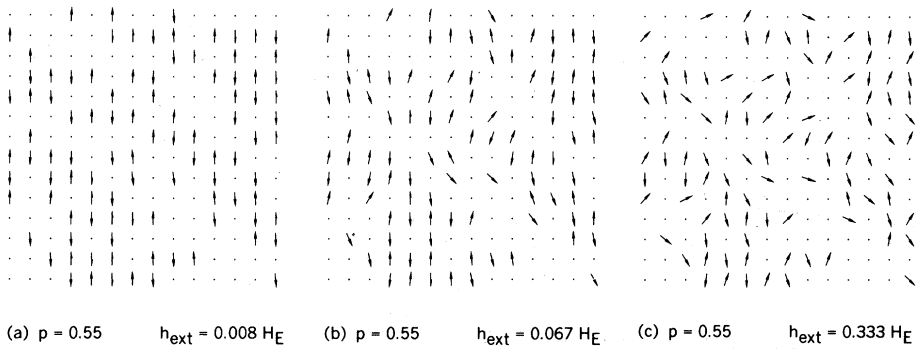

FIG. 16. Equilibrium spin orientations as in Fig. 15, but for one layer in a $14\times14\times14$ sample with concentration = 0.55 and h_{ext}/H_E = 0.008 in (a), = 0.067 in (b), and = 0.33 in (c).

for which $\vec{q}$ lies along the easy axis and a field is applied perpendicular to $\vec{q}$. In a pure system, the only magnetic contribution to the elastic scattering will be a small additional amplitude of the ferromagnetic Bragg peaks. In contrast, in the random system, as illustrated in Figs. 15 and 16, the staggered magnetization is pulled away from the easy axis in the ferrimagnetic regions. Thus, locally one obtains a staggered magnetization perpendicular to $\vec{q}$. This local order persists over distances which are governed by the connectivity of the dilute network. Accordingly, the field-induced superlattice reflections will have a width proportional to ξ^{-1}, where ξ is the physical distance between nodes introduced in Sec. VIII. Thus ξ can be measured by neutron diffraction.

X. RESULTS FOR GARNETS

In this section we present numerical results[9] for randomly diluted or mixed garnets. Per unit cell, all the garnets which we will consider can be represented by the formula

$$4\{[\mathrm{Fe}_{2-x}M_x][\mathrm{Fe}_{3-y}M_y][R_{3-z}S_z]\mathrm{O}_{12}\}, \qquad (149)$$

where M represents one or more trivalent nonmagnetic ions substituted for the iron ions and R and S are both trivalent rare earths, or one may be yttrium. The grouping of ions in square brackets in (149) indicates the relative occupation within the a, d, and c sublattices. Pure YIG is described by $x=y=z=0$ with R being yttrium, which is nonmagnetic. The systems described by (149) can be prepared over almost the entire range of the parameters x, y, and z.[4,60-62] Nonmagnetic alkaline-earth ions are also commonly substituted for Y in order to reduce the net lattice constant changes when the Fe ions are replaced by ions of very different size. Since this introduces no new magnetic phenomena, we shall ignore this possibility. We will first present results for diluted YIG where R = Y and $z=0$. Subsequently, we treat rare-earth garnets in which R and S are magnetic.

For dilute YIG we show in Fig. 17 the percolation threshold as a function of the fraction of vacancies on the d (majority) sublattice. The threshold occurs at the highest net Fe concentrations when substitution is confined to a single sublattice. That is, Fig. 17 shows that to disconnect the system requires the removal of 1.6 of the two Fe ions on the a sublattice, leaving a net Fe concentration of 68 at.%, or 2.6 out of 3 Fe ions on the d sublattice, leaving 48 at.%. For substitution of nonmagnetic ions into Fe sites with no preference for either sublattice the critical Fe concentration is 40 at.%. Thus, we conclude that subsititution confined to a single sublattice produces more drastic effects than completely random substitution.

We next show, in Figs. 18–21, A as a function of composition for various types of dilution in YIG. It is believed[61,63-66] that $J_{dd}/J_{ad} \approx J_{aa}/J_{dd} \approx 0.1$. In Fig. 18, we show that the effect of including the second-neighbor interaction J_{dd} on $A(x,y)/A(2,3)$

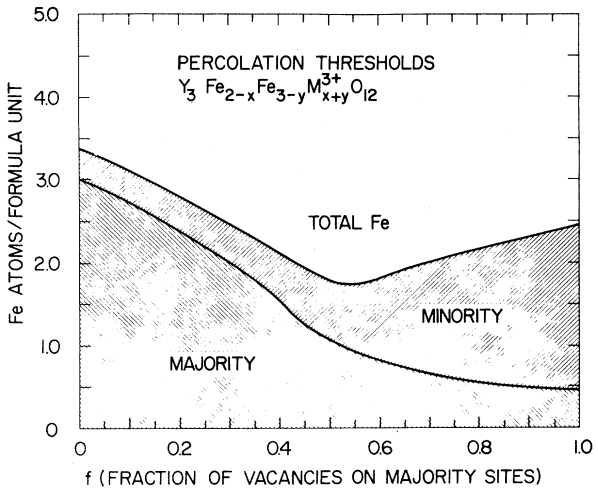

FIG. 17. Percolation threshold for the dilute garnet system. The vacancy concentration is $\frac{1}{2}x$ on a sites and $\frac{1}{3}y$ on d sites, while $f = y/(x+y)$ is the fraction of the vacancies which are on the d sublattice. The shaded areas represent the number of sites (per formula unit) occupied at threshold on the majority (d) or minority (a) sublattice.

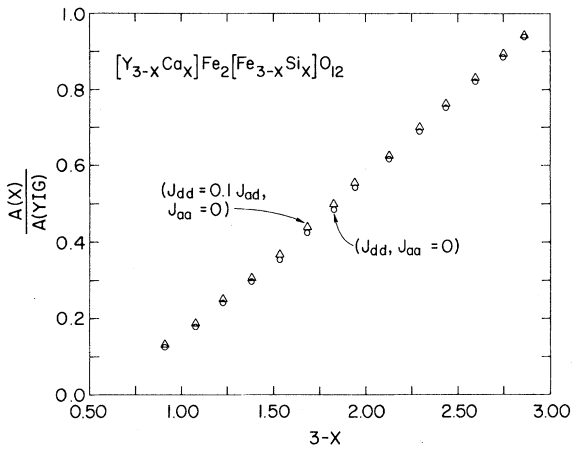

FIG. 18. $A(y)$ vs $3-y$ for YIG diluted only on the majority sublattice. The circles were calculated under the approximation $J_{aa}=J_{dd}=0$, while the triangles show the effect of introducing next-nearest-neighbor interactions ($J_{dd}/J_{ad}=0.1$, $J_{aa}=0$). Calculations in this and the following four figures were made on samples with 7000 Fe sites.

is quite small in the case where substitution occurs on the majority sublattice only. This is the case in which the effect of J_{dd} should be slightest, since every d sublattice ion remaining has a full complement of a sublattice neighbors. The effect remains small for small dilution even when equal fractions of the Fe sites on the two sublattices are substituted, the case depicted in Fig. 19. J_{dd} affects the stiffness in a more drastic way by causing the Néel state to be unstable whenever a d ion has no a neighbors. This occurred whenever $x+y>1$ in the case of Fig. 19, and at all concentrations considered for substitution on the minority sublattice only, shown in Fig. 20. This observation is consistent with the suggestions of Rosencwaig[67] and Geller,[68] that random canting takes place on the sublattice with the smaller number of vacancies. Since this presumably affects only a small number of sites, and the effect of J_{dd} was found to be small until the instability occurs, we have taken $J_{dd}=J_{aa}=0$ in the cases shown in Figs. 19–21, and do not attempt to model any random canting.

Also shown in Figs. 19–21 is the behavior of the spin-wave stiffness D, calculated by $D(x)\propto A(x)/M(x)$, where $M(x)$ is obtained by taking the Néel state magnetization for spins in the infinite cluster. In Fig. 21 we have used the actual 90% d-sublattice preference found[69] for Ga substitution of 30% or less. Since the magnetization passes through zero at a compensation point in this case, D increases with dilution, and changes sign. (The absolute value of D is plotted in Fig. 21.) The behavior of the spectrum at long wavelengths close to such a compensation point is studied in more detail below.

These calculations of $A(x)$ for Ga substitution may be compared with available measurements of spin-wave resonance at room temperature.[70] In making this comparison it is important to realize that T_c also depends on Fe concentration, and that this is

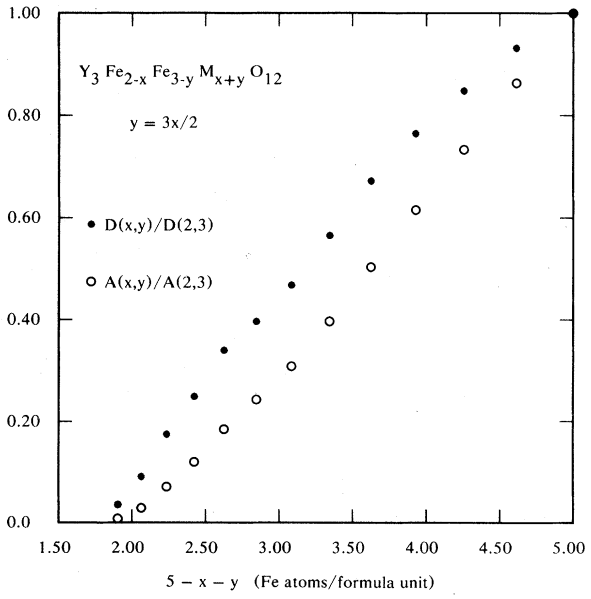

FIG. 19. Exchange stiffness $A(x, y)$ for YIG, plotted as a function of total Fe concentration, for the case when dilution occurs with equal probability on the two sublattices. Only nearest-neighbor interactions (J_{ad}) were included. The spin-wave stiffness, $D(x, y)$, is indicated by the solid data points.

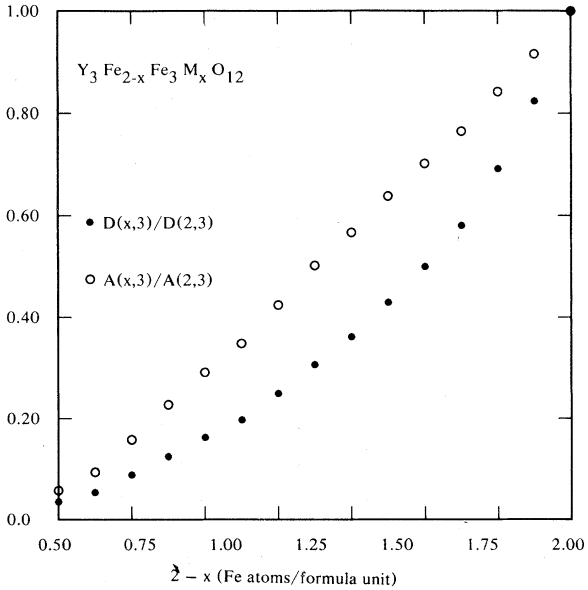

FIG. 20. $A(x)$ and $D(x)$ vs $2-x$ as in Fig. 19, but for dilution on the minority sublattice only.

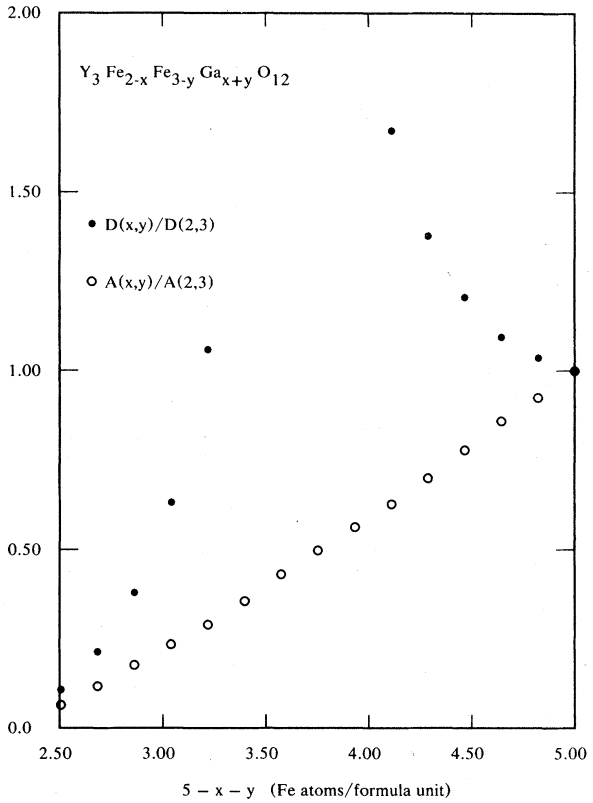

FIG. 21. A and D versus total Fe concentration as in Fig. 19, but for $y/x=8$, the ratio applicable to most Ga-doped YIG samples at moderate vacancy concentrations (Ref. 69).

the dominant source of composition dependence in the value of A at room temperature.[45] The theory of Ref. 45 can be improved by using the zero-temperature dependence of A on concentration from our numerical work, as is described in Ref. 9, and very close agreement is achieved. However, no existing theory can explain the unusual temperature dependences reported by Enoch *et al.*[71]

Our result for $A(x,y)$ are usefully summarized by the approximate empirical formula

$$A(x,y)/A(2,3)=1-0.73x-0.43y+0.25xy, \quad (150)$$

and are plotted in Fig. 22 vs b, the fraction of bonds which are present:

$$b=(1-\tfrac{1}{2}x)(1-\tfrac{1}{3}y)$$
$$=1-\tfrac{1}{2}x-\tfrac{1}{3}y+\tfrac{1}{6}xy. \quad (151)$$

Since the coefficients of x, y, and xy in (150) are in nearly the same ratios as in (151), the points in Fig. 22 fall close to a universal curve. In contrast, if the data of Figs. 18–21 are plotted versus the fraction of missing sites, four distinct curves result. In Fig. 22 we also observe that $A(x,y)$ varies nearly linearly with bond concentration,[41]

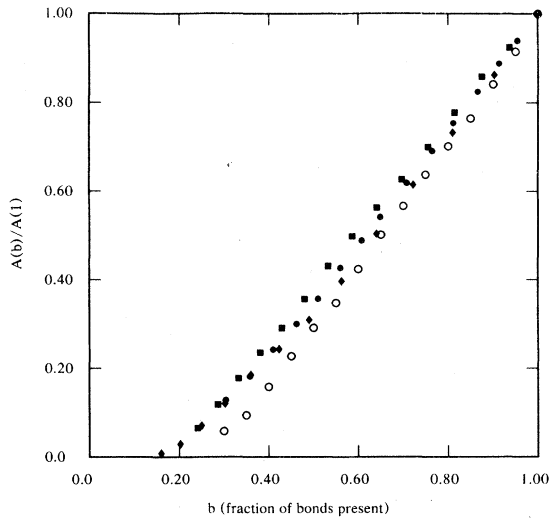

FIG. 22. Exchange stiffness A (data of Figs. 18–21) plotted versus b, the fraction of bonds which are present. The cases plotted are doping on the minority sublattice only (circles), doping with the same probability on both sublattices (diamonds), Ga substitution (squares), and dilution of the majority sublattice only (points).

while it is a nonlinear function of site occupation when both sublattices are substituted, as Fig. 19 demonstrates.

Finally, the behavior of $A(x,y)$ for nearly pure YIG can be understood qualitatively using the results for cubic systems. We use the result, based on the approximation (91) that

$$A^{-1}\left(\frac{dA}{dc}\right)_{c=0}-2\sim\frac{2}{z-1}, \quad (152)$$

when nonmagnetic ions are substituted without preference for either sublattice. For the garnet lattice $z=6$ for a sites and 4 for d sites. Therefore, $(A^{-1}\,dA/dc-2)$ is expected to be slightly larger for garnets than for the sc lattice. To estimate it for garnets, we assume that $(A^{-1}\,dA/dc-2)$ is proportional to $(z-1)^{-1}$ and scale the sc result accordingly, using $z\sim5$ for the garnets:

$$A^{-1}\frac{dA}{dc}\sim2+\frac{5}{4}\left(A_{sc}{}^{-1}\frac{dA_{sc}}{dc}-2\right)\sim2.66. \quad (153)$$

Our results, as summarized in (150), yield $A^{-1}\,dA/dx\sim0.73$, and $A^{-1}\,dA/dy\sim0.43$ in the low-dilution limit. Thus, for $\frac{1}{2}x+\frac{1}{3}y=c$ we obtain $A^{-1}\,dA/dc=2.7$, in agreement with our theoretical estimate.

It has been suggested on empirical grounds[45] that the variation of T_c with dilution can be related to that of A by

$$T_c(x,y)/T_c(2,3)=A(x,y)/A(2,3), \quad (154)$$

where A is the zero-temperature stiffness. As we have seen in Table II, this relation does not hold

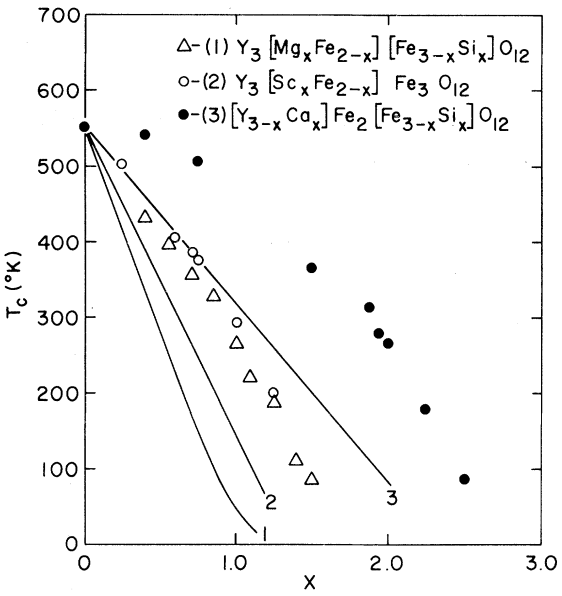

FIG. 23. Comparison of the measured (Ref. 4) T_c for three substituted YIG series and the values T_c would take (solid lines) if it were proportional to A.

even qualitatively for simple lattices. For the garnets this relation is more reasonable, but still is not satisfactory, as can be seen from Fig. 23, where we compare experimental values of $T_c(x,y)/T_c(2,3)$ with our numerical results for $A(x,y)/A(2,3)$. Clearly, it would be useful to have experimental values of the latter quantity to corroborate our calculations.

The lowest-energy long-wavelength modes in diluted YIG can be treated by the continuum approximation (32), which predicts two modes. Of particular interest is the case when dilution occurs predominantly on the d sublattice, so that $M(x) = M_d(x) - M_a(x) \sim 0$.[60-62] The two effects of dilution we wish to illustrate are (i) as $M(x) \to 0$, the frequency of the optical (exchange) mode vanishes, and (ii) when $M(x) \sim 0$ the dispersion relation shows both $\omega \propto q$ and $w \propto q^2$ regimes. To

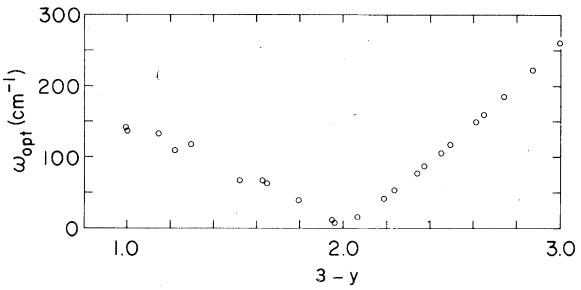

FIG. 24. Optical-mode frequency for Si-doped YIG (dilution only on the d sublattice) calculated from (33) using Monte Carlo data for $\chi_\perp$ and $M_d - M_a$.

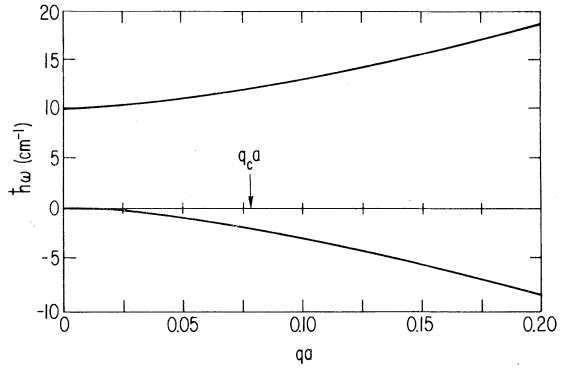

FIG. 25. Dispersion relations for the acoustic and low-energy optical mode for Si-doped YIG near compensation as calculated from (32). For $q \ll q_c$, where q_c is defined in (36), the frequencies vary as q^2; for $q \gg q_c$ they vary as q.

study the optical-mode frequency we have calculated $\chi_\perp$ and M for dilution only on the d sublattice, as is thought to occur in Si substitution.[4] Compensation occurs at $T=0$ when $y \approx 1$, since $M_d(y) \sim (1 - \frac{1}{3}y)M_d(1)$ this far above the percolation threshold. The predicted $\omega_{opt}(y)$ is plotted in Fig. 24. The curve is asymmetric about $y=1$ because $\chi_\perp(y)$ increases more rapidly below $y=1$ than above. At compensation, $\chi_\perp(y) \sim 1.1\chi_\perp(0)$. To exhibit the changeover in ω from linear to quadratic dependence on q, we study a case in which $\omega_{opt} \sim 10$ cm^{-1}. This will occur for $y \sim 1.95$ or 2.05, and is plotted in Fig. 25. For either choice of composition, crossover should be observed at $q_c a \sim 0.08$.

We next consider mixed rare-earth iron garnets. Here a simple two-sublattice model can again be used, at low energies, since the Fe-Fe exchange interactions are much stronger than the Fe-R terms. In this model we treat only excitations in which all iron spins precess nearly in phase. Likewise, all rare-earth spins are considered to precess in concert. There will also be excitations in which rare-earth spins are incoherently excited at the single-ion frequency, ω_{si}, given by[72,73]

$$\hbar\omega_{si} = |4J_{dc} - 8J_{ac}|S_{Fe} = \Delta_{si}S_{Fe}, \qquad (155)$$

where $S_{Fe} = \frac{5}{2}$ is the iron spin and we assume that J_{dc} and J_{ac} are both negative (antiferromagnetic) couplings. In a garnet containing two species of rare-earth ions having sufficiently different values of ω_{si} we expect to find two bands of incoherent single-ion excitations. The energies we are considering are low enough that only the lowest acoustic mode of YIG, shown in Fig. 26(c), will be relevant to alloys of YIG with rare-earth ions.

Tinkham[74] has treated excitations in pure YbIG in this spirit. His approach leads to a 2 by 2 secular determinant, with exchange terms $\Delta_{si}S_{Fe}$ or $\Delta_{si}S_R$ coupling the Yb and Fe sublattices. Since

J_{cd} and J_{ca} are negligible in comparison with J_{ad}, A is the same as in pure YIG, and a stiffness term $D_{\mathrm{YIG}}q^2$ appears in the Fe-Fe element of the secular determinant. The secular equation can be written

$$\omega^2 - \omega[\omega_{si}(S_d - S_a - S_c)/(S_d - S_a) - D_{\mathrm{YIG}}q^2] - \omega_{si}D_{\mathrm{YIG}}q^2 = 0, \quad (156)$$

where S_d, S_a, and S_c are the spin per unit cell on the d, a, and c sublattices, respectively. $S_d = 12(\frac{5}{2}) = 30$, $S_a = 8(\frac{5}{2}) = 20$, and for GdIG $S_c = 12(\frac{7}{2}) = 42$. For YbIG, $S_c = 6$, since the Yb^{3+} ions is in a Kramers doublet[75] with $S_{\mathrm{eff}} = \frac{1}{2}$. The two branches obtained using (156) for GdIG and YbIG are shown in Figs. 26(a) and 26(b). For completeness we have also indicated the presence of incoherent excitations of the rare-earth spins at frequency ω_{si}. Equation (156) is the analog of (32) if the definition of γ given in (14) is used. The only difference between (156) and (32) is that in the former a term $-\omega D_{\mathrm{YIG}}q^2$ is included. This term is unimportant in the hydrodynamic regime, but insures that one root of (156) will tend to ω_{si} at large q. For small q the acoustic mode obtained from (156) is

$$\omega = -Dq^2 = -D_{\mathrm{YIG}}q^2(S_d - S_a)/(S_d - S_a - S_c), \quad (157)$$

and has the correct dependence on total spin given by (13b) and (14), as has been noted previously.[76] For $S_d - S_a - S_c > 0$, D is positive and an acoustic spin wave tends to decrease $S_d - S_a$. This is the case in YIG or YbIG, shown in Fig. 26. For $S_d - S_a - S_c < 0$, D is negative and an acoustic spin wave tends to increase $S_d - S_a$, as occurs in GdIG (Fig. 26).

The optical mode at $q = 0$ is given by (156) as

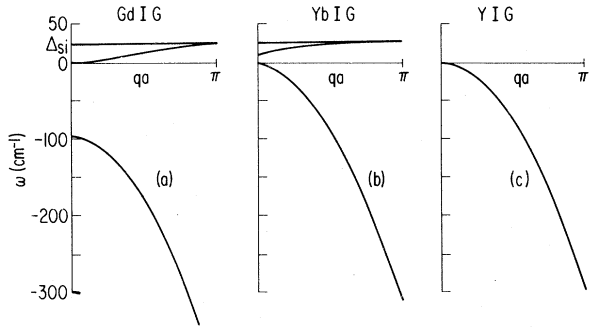

FIG. 26. The low-energy region of the spin-wave spectrum of various pure garnets. The incoherent excitations on the rare-earth sublattice (in GdIG and YbIG) give rise to a spin-wave band centered at the single-ion exchange energy, Δ_{si}. The other modes in GdIG and YbIG, arising from the coupled motion of the two sublattices, have frequencies determined by (156). For YIG, this model yields a single spin-wave branch whose dispersion is given by (157) with $S_c = 0$.

$\omega = \omega_{\mathrm{opt}}$ with

$$\hbar\omega_{\mathrm{opt}} = \hbar\omega_{si}(S_d - S_a - S_c)/(S_d - S_a). \quad (158)$$

We can now make contact with Tinkham's work, which reproduces the original formula of Kaplan and Kittel[16,20] for a two-sublattice system, viz.

$$\omega_{\mathrm{opt}} = \lambda(\gamma_1 M_2 - \gamma_2 M_1), \quad (159)$$

where λ is an exchange constant and γ_i and M_i are the gyromagnetic ratio and magnetization of the ith sublattice. This notation makes it appear that ω depends on γ_i. However, as we have previously noted, ω is independent of the g values. We can rewrite (33) in the form,

$$\hbar\omega_{\mathrm{opt}} = \mu_B^2(S_d - S_a - S_c)/(\chi_\perp^{ss} v_0), \quad (160)$$

where $\chi_\perp^{ss}$ is the spin-spin susceptibility defined in I as the susceptibility evaluated for unit g values, and v_0 is the volume of the unit cell containing 12 d sites. One can show that $\chi_\perp^{ss}$ is

$$\chi_\perp^{ss} = \mu_B^2(S_d - S_a)/(\hbar\omega_{si} v_0), \quad (161)$$

which shows that (160) and (158) are equivalent.

We now present some results for mixed rare-earth–iron garnets. We assume that all the iron sites are occupied and characterize the rare-earth sublattice by its spin density S_c. For YbIG,[72,77] $\hbar\omega_{si} = 25.0\ \mathrm{cm}^{-1}$, and for GdIG,[72,78] $\hbar\omega_{si} = 27.8\ \mathrm{cm}^{-1}$, so the approximation of treating the two types of rare-earth ions as a single sublattice should be reasonably good in {Yb-Gd}IG.

As $|S_d - S_a - S_c|$ is decreased, for example, by appropriate dilution, $\hbar\omega_{\mathrm{opt}}$ becomes small. The evolution of the spin-wave spectrum versus concentration for mixed {Yb-Gd}IG is shown in Fig. 27. In this connection it is interesting to note that the zero-spin condition $S_c = S_d - S_a$ does not imply

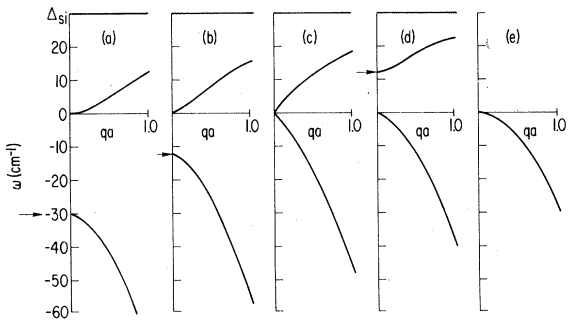

FIG. 27. Low-energy regions of the spin-wave spectrum for some mixed garnets, with the formula $[Yb_x Gd_{1-x}]_3Fe_5O_{12}$, in panels a–d and for pure YIG in panel e. In case c, spin compensation occurs, and for both acoustic branches $\omega \propto q$. The optical mode, whose frequency at $q = 0$ is given by (158), is indicated by an arrow.

zero magnetization, since the g values of the rare-earth ions are not equal to the g value of iron. Indeed, pure YbIG is an antiferromagnet in the sense that its magnetization is very nearly zero at $T=0$. However, its spin-wave spectrum is ferromagnetic with a single acoustic mode with $\omega_q \propto q^2$ [Fig. 27(d)]. By contrast, $Fe_5(Gd_zYb_{1-z})_3O_{12}$, with $z=\frac{1}{9}$ has zero-effective spin, and therefore an antiferromagnetic spectrum in the sense that the acoustic mode is twofold degenerate and has $\omega_q \propto q$ [Fig. 27(c)], but has nonzero magnetization. In this case, for small q, i.e., for $Dq^2 < \hbar\omega_{si}$ one has

$$\hbar\omega_q = \pm(\hbar\omega_{si}D)^{1/2}aq - \tfrac{1}{2}Da^2q^2 . \tag{162}$$

A particularly interesting question is raised by the possible occurrence of well-defined optical modes in such mixed systems. Are these optical modes well defined at all concentrations, or is our continuum treatment restricted to certain ranges of concentration? The clearest answer to this question will probably come from experiment, since these modes are observable by infrared spectroscopy.[74,77]

XI. SUMMARY AND CONCLUSIONS

(i) In the limit of small anisotropy, the hydrodynamic picture of spin waves first introduced by Halperin and Hohenberg[13] gives useful predictions for disordered ferromagnets, ferrimagnets, and antiferromagnets. The frequencies of the elementary excitations at long wavelengths and low energies are given by

$$\omega_q = \omega_0 + Dq^2 \tag{12}$$

for ferro- and ferrimagnets, and by

$$\omega_q^2 = \omega_0^2 + C^2q^2 \tag{18}$$

for antiferromagnets, where D and C are related to the static magnetic elastic constants A, the exchange stiffness, $\chi_\perp$, the perpendicular susceptibility, and M, the average magnetization per unit volume, by $D=2\gamma A/M$ and $C^2=2\gamma^2A/\chi_\perp$, where γ is the gyromagnetic ratio.

In this paper, we have evaluated A, $\chi_\perp$, and M for various random dilute magnets at arbitrary defect concentrations. The elastic constants were then used in the hydrodynamic framework or extensions thereof to discuss elementary excitations. We have confined our examples to dilute systems in this paper because these are the most difficult for conventional "average-medium" theories to treat.[17,30] Applicability of these methods to a two-component antiferromagnetic alloy has also been demonstrated in a previous paper.[17]

(ii) We have carried out an exact calculation of the effects of a single defect in order to estimate the errors resulting from the use in (12) and (18) of the hydrodynamic expressions for D and C (in terms of static elastic constants) when the gap frequency ω_0 is finite. Use of the static parameters leads to errors in the gap frequency and in $(d\omega/dq^2)_{q=0}$ of order ω_0/ω_E, where ω_E is the exchange frequency.

(iii) For high concentrations of defects, for more elaborate types of disorder, or for materials with complex crystal structures, the magnetic elastic constants can be obtained numerically by a simulation method. We have calculated $M(p)$, $A(p)$, and, for antiferromagnets, $\chi_\perp(p)$, for the planar-square, simple cubic, body-centered-cubic, and garnet lattices. These calculations reproduce the results of the single defect theory as $p \to 1$, except in the case of garnets, for which no single defect results are available.

(iv) The static elastic constants display critical behavior near χ_c, the critical concentration for percolation. We have obtained estimates of the exponents characterizing this region for the square and simple cubic lattices. Inequalities relating these exponents to the exponents occurring in the more conventional percolation cluster statistics problem have also been obtained. The critical dimensionality for the onset of mean-field behavior in the elastic constants is found to be 6, as is also true for the static cluster properties.[47,53]

(v) We have shown that configurational fluctuations cause $\chi_\perp$ in an isotropic antiferromagnet to diverge (i) as $p \to p_c$, and (ii) in two or fewer spatial dimensions for all $p \neq 1$. In both cases the divergence results from local fluctuations in the total spin which are present because the two sublattices in a randomly diluted antiferromagnet are not balanced microscopically. Anisotropy removes the divergence in both cases, but a prominent maximum in $\chi_\perp$ persists at x_c. As a consequence of the type (ii) divergence, $\omega \propto q/(\ln q)^{1/2}$ as $q \to 0$ in an isotropic two-dimensional dilute antiferromagnet.

(vi) We propose two experiments in antiferromagnets to observe configuration fluctuation which give rise to locally ferromagnetic regions. The induced hyperfine field at the nucleus of a nonmagnetic impurity will be broadened by the application of a transverse magnetic field. Elastic neutron scattering in the presence of a transverse field can sense the magnitude and length scale of these fluctuations.

(vii) We have studied the nonlinear response of dilute antiferromagnets to an external field perpendicular to the easy axis. This calculation reproduces the field-dependence seen by Breed *et al.*[2] in dilute 2D and 3D systems. The principal cause of the nonlinearity is a breakdown of the usual small-angle approximation which occurs when the ferrimag-

netic fluctuations approach saturation.

(viii) Dilution of a ferrimagnet predominantly on its majority sublattice can create an antiferromagnet. The crossover from ferri- to antiferromagnetic behavior can be studied in a continuum approximation which is a natural extension of (12) and (18). At concentrations close to the compensation point there exists a spin-wave optical mode whose frequency is proprotional to the unbalanced spin density. For dilute YIG the variation of the optical mode frequency with dilution, shown in Fig. 24, should be observable by infrared absorption measurements of the type done by Sievers and Tinkham[77] on pure YbIG.

We also propose study of dilute {Yb-Gd}IG to explore the details of this crossover (see Fig. 27). These alloys have the interesting feature that angular momentum compensation occurs at a different Yb concentration than does magnetization compensation. Thus one can study a system whose elementary excitations resemble those of an antiferromagnet, but which has an appreciable net magnetic moment.

ACKNOWLEDGMENTS

The authors gratefully acknowledge useful discussions with B. I. Halperin, T. C. Lubensky, and W. P. Wolf.

APPENDIX A: MICROSCOPIC DERIVATION OF LONG-WAVELENGTH BEHAVIOR

In Sec. III we gave a continuum derivation of the formula for the frequency of long-wavelength spin waves in terms of static response functions. That formulation coincides with the hydrodynamic treatment, and therefore should give correctly the frequencies of hydrodynamic or first spin waves. This regime is characterized by $\omega\tau \ll 1$, where τ is a thermal relaxation time. However, since $\tau \to \infty$ as the temperature T goes to zero, one enters the opposite regime, $\omega\tau \gg 1$, for fixed ω as $T \to 0$. Then the elementary excitations are mechanical or zero-spin waves, our terminology being analogous to that of zero and first sound in a phonon gas. In this appendix we study the zero-temperature excitations from a microscopic point of view, and obtain results which agree with the hydrodynamic formulation. This equivalence is expected to obtain only in the zero-temperature limit.

We will discuss the dilute ferri- and antiferromagnets by relating their microscopic equations of motion to those of the ferromagnet, and thereby make contact with the analysis of Brenig *et al.*[21] They studied the random system

$$\sum_j N_{ij} x_j^{(n)} = \omega^{(n)} x_i^{(n)} , \tag{A1}$$

where

$$N_{ij} = p_i \sum_d (\delta_{i,j} p_{i+d} - \delta_{j,i+d} p_j) , \tag{A2}$$

where d is summed over nearest neighbors of i. The matrix $\underline{N}$ is a conductance matrix because it has the properties

$$\sum_j N_{ij} = 0 , \tag{A3a}$$

$$N_{ij} = N_{ji} . \tag{A3b}$$

Note that there are eigenvector(s) corresponding to $\omega^{(n)} = 0$ which involve solutions $x^{(n)}$ uniform over a cluster. The uniform solution over the infinite cluster is denoted $x^{(0)}$:

$$x_j^{(0)} = \begin{cases} N^{-1/2} & (j \in \infty) , \qquad \text{(A4a)} \\ 0 & (j \notin \infty) , \qquad \text{(A4b)} \end{cases}$$

where N is the number of sites in the infinite cluster. According to Brenig,[21] there are solutions $x^{(n)}$ with eigenvalues $\omega^{(n)}$ which we may write in the low-frequency limit as $x^{(k)}, \omega^{(k)}$, where k is a momentum vector of the first Brillouin zone and

$$\omega(k) = Da^2k^2 . \tag{A5}$$

The dispersion constant D is related to the conductivity σ of the randomly diluted network by

$$\frac{D}{D_{\text{pure}}} = \frac{\sigma}{\sigma_{\text{pure}}} \frac{\sum_j \mathbf{1}}{\sum_j p_j} , \tag{A6}$$

where here and below p_j is 1 if $j \in \infty$, and is zero otherwise. Here the subscript pure indicates the value for the pure system. It is easy to show that $\sigma/\sigma_{\text{pure}} = A/A_{\text{pure}}$, where A is the exchange stiffness introduced in Sec. III. Also, if there is no canting, $\sum_j p_j = M(p)/M(1)$, in which case (A6) is equivalent to (13b).

Now we apply these ideas to the ferrimagnet. Here the equations of motion are

$$\hbar\omega S_i^+ = \left(\sum_j 2J_{ij} S_j^z \right) S_i^+ - 2 \sum_j J_{ij} S_i^z S_j^+ . \tag{A7}$$

We will work at $T = 0$ and neglect spin-wave interactions. Then $S_i^z = \pm S_i$, the sign depending on the sign of S_i^z in the Néel state. For the random ferrimagnet (or ferromagnet) we set $J_{ij} = 0$ if either site i or site j is vacant, and we use (A7) only for spins in the infinite cluster. We write (A7) as

$$\hbar\omega S_i^+ = \sum_j M_{ij} S_j^+ , \tag{A8}$$

where

$$M_{ij}=\left(\sum_k J_{ik}S_k^z\right)\delta_{ij}-J_{ij}S_i^z. \tag{A9}$$

Note that $\underline{M}$ is not symmetric and can not yet be identified as the conductance matrix of a random network. We denote the eigenvectors of $\underline{M}$ by $|\psi_n\rangle$:

$$\underline{M}|\psi_n\rangle=\hbar\omega_n|\psi_n\rangle, \tag{A10a}$$

$$\langle\psi_n|\underline{M}=\hbar\omega_n\langle\psi_n|. \tag{A10b}$$

Note that $\langle\psi_n|$ is not the transpose of $|\psi_n\rangle$ because $\underline{M}$ is not symmetric. In particular, we have

$$M_{ij}S_j^z=M_{ji}S_i^z, \tag{A11}$$

so that if

$$\sum_j M_{ij}|\psi_n\rangle_j=\hbar\omega_n|\psi_n\rangle_i, \tag{A12a}$$

then

$$\sum_j M_{ji}(S_i^z/S_j^z)|\psi_n\rangle_j=\hbar\omega_n|\psi_n\rangle_i \tag{A12b}$$

or

$$\sum_j M_{ji}[(S_j^z)^{-1}|\psi_n\rangle_j]=\hbar\omega_n(S_i^z)^{-1}|\psi_n\rangle_i. \tag{A12c}$$

Thus

$$\langle\psi_n|_j=|\psi_n\rangle_j/S_j^z \quad (j\in\infty), \tag{A13a}$$

$$=|\psi_n\rangle_j=0 \quad (j\notin\infty). \tag{A13b}$$

Here $|\psi_n\rangle_j$ and $\langle\psi_n|_j$ are the jth components of the vectors $|\psi_n\rangle$ and $\langle\psi_n|$. We normalize $|\psi_n\rangle$ by

$$\langle\psi_n|\psi_n\rangle=\pm1 \tag{A14a}$$

or

$$\sum_j p_j(|\psi_n\rangle_j)^2/S_j^z=\pm1. \tag{A14b}$$

The $q=0$ (i.e., uniform) eigenvector is found using Eq. (A9) to be

$$|\psi_0\rangle_j=p_jS_j^z\Big/\left|\sum_j p_jS_j^z\right|^{1/2}, \tag{A15a}$$

$$\langle\psi_0|_j=p_j\Big/\left|\sum_j p_jS_j^z\right|^{1/2}. \tag{A15b}$$

To relate the spin-wave problem to a network we define

$$N_{ij}=M_{ij}S_j^z. \tag{A16}$$

Now $\underline{N}$ satisfies Eq. (A3) and is therefore a conductance matrix. If the eigenvectors of $\underline{N}$ are $|\varphi_n\rangle$, then we may write

$$\underline{N}|\varphi_n\rangle=\lambda_n|\varphi_n\rangle, \tag{A17a}$$

$$\langle\varphi_n|\underline{N}=\langle\varphi_n|\lambda_n, \tag{A17b}$$

where $\langle\varphi_n|$ is the transpose of $|\varphi_n\rangle$. Also we have

$$\underline{N}=\sum_n|\varphi_n\rangle\lambda_n\langle\varphi_n|. \tag{A18}$$

In particular, $\underline{N}|\varphi_0\rangle=0$ with

$$|\varphi_0\rangle_j=p_j\Big/\left(\sum_j p_j\right)^{1/2}. \tag{A19}$$

From Eq. (A15) we see that

$$\underline{M}=\underline{N}\underline{S}^{-1}, \tag{A20}$$

where

$$S_{ij}=\delta_{ij}S_i^z. \tag{A21}$$

Using (A18) and (A20) we obtain

$$\underline{M}=\sum_n|\varphi_n\rangle\lambda_n\langle\varphi_n|\underline{S}^{-1}. \tag{A22}$$

Thus the eigenvalue condition for the spin-wave energies is

$$\sum_n|\varphi_n\rangle\lambda_n\langle\varphi_n|\underline{S}^{-1}|\psi_j\rangle=\hbar\omega^{(j)}|\psi_j\rangle. \tag{A23}$$

Multiplying on the left by $\langle\varphi_r|$, we obtain

$$\lambda_r\langle\varphi_r|\underline{S}^{-1}|\psi_j\rangle=\hbar\omega^{(j)}\langle\varphi_r|\psi_j\rangle. \tag{A24}$$

Now in the limit $\lambda_r\to0$, Brenig *et al.*[21] find that q becomes a good quantum number, and therefore we may label the eigenvectors and eigenvalues by momentum q and write

$$\omega_q=Da^2q^2, \tag{A25}$$

$$\lambda_q/\hbar=D^*a^2q^2. \tag{A26}$$

Here D and D^* and the spin-wave dispersion constants for the original system described by $\underline{M}$ and that for the modified system described by $\underline{N}$, respectively. Brenig *et al.*'s formulation for the ferromagnet enables us to determine D^*. It remains to relate D to D^*. This is done by using (A24):

$$D^*\langle\varphi_q|\underline{S}^{-1}|\psi_q\rangle=D\langle\varphi_q|\psi_q\rangle. \tag{A27}$$

Now we take the limit $q\to0$ and obtain

$$D=D^*\langle\varphi_0|\underline{S}^{-1}|\psi_0\rangle/\langle\varphi_0|\psi_0\rangle. \tag{A28}$$

Using (A15) and (A19) we evaluate this as

$$D=D^*\sum_j p_j\Big/\sum_j p_jS_j^z. \tag{A29}$$

Finally we relate D^* to the stiffness (or conductivity) A of the lattice governed by $\underline{N}$ according to (A6):

$$\frac{D^*}{D^*_{\text{pure}}}=\frac{A^*}{A^*_{\text{pure}}}\frac{\sum_j 1}{\sum_j p_j}. \tag{A30}$$

Here A^* is the stiffness corresponding to $\underline{N}$, i.e.,

it is proportional to the conductivity of the network described in (46). A^* is also the exchange stiffness for the original system described by (A7). Combining (A29) and (A30) we obtain the desired relation

$$D(p)/D(1) = [A^*(p)/A^*(1)]\left(\sum_j S_j^z(1)\Big/\sum_j p_j S_j^z(p)\right). \tag{A31}$$

where $S_j^z(1)$ denotes the value of S_j^z in the Néel state of the pure system and $S_j^z(p)$ is the value of S_j^z at equilibrium for the dilute system. From the discussion following (A16), it is clear that $S_j^z(p)$ will only differ from $S_j^z(1)$ if there exist clusters coupled to the infinite cluster by competing interactions. Equation (A31) agrees with (13b) and with the hydrodynamic result.

Next we consider the randomly diluted antiferromagnet. We shall study a two-sublattice system with nearest-neighbor exchange interactions between "up" spins on the a sublattice and "down" spins on the b sublattice. We write (A7) for this case as

$$\tilde{\omega} S_{ia}^+ = \left(\sum_k J_{ik}\right) S_{ia}^+ + \sum_k J_{ik} S_{kb}^+ , \tag{A32a}$$

$$\tilde{\omega} S_{jb}^+ = -\left(\sum_l J_{jl}\right) S_{jb}^+ - \sum_l J_{jl} S_{la}^+ . \tag{A32b}$$

Here S_{ia}^+ and S_{jb}^+ denote spin operators for the sites i (on the a sublattice) and j (on the b sublattice), respectively, $\tilde{\omega}$ denotes $\hbar\omega/2S$, and we absorb the sign of J, letting J_{ij} denote $|J_{ij}|$. To identify these equations with those of a network we eliminate S_{jb}^+:

$$S_{jb}^+ = -\sum_i \frac{J_{jl} S_{la}^+}{\tilde{\omega} + J z_j} , \tag{A33}$$

where z_j is the number of nearest neighbors of j: $J z_j = \sum_m J_{jm}$. Inserting this into (A32a) we obtain

$$\tilde{\omega} S_{ia}^+ = J z_i S_{ia}^+ - \sum_{kl} \frac{J_{ik} J_{kl} S_{la}^+}{\tilde{\omega} + J z_k} . \tag{A34}$$

We write this as

$$\tilde{\omega}\left(p_i - \sum_k \frac{J_{ik}}{\tilde{\omega} + J z_k}\right) S_{ia}^+ = \sum_j \left(\frac{1}{2S}\right) T_{ij} S_{ja}^+ , \tag{A35}$$

where

$$\left(\frac{1}{2S}\right) T_{ij} = \left(\sum_{kl} \frac{J_{ik} J_{kl}}{\tilde{\omega} + J z_k}\right) \delta_{ij} - \sum_k \frac{J_{ik} J_{kj}}{\tilde{\omega} + J z_k} . \tag{A36}$$

Note that since $\underline{T}$ satisfies (A3) it can be regarded as the conductance matrix of a network defined on the a sublattice only. The conductances T_{ij} depend upon atoms occupying both a and b sites. To order ω^2 we expand (A35) as

$$\left[(\hbar\omega)^2 \sum_k \frac{J_{ik}}{2J^2 S z_k^2} + (\hbar\omega)\left(p_i - \sum_k \frac{J_{ik}}{J z_k}\right)\right] S_{ia}^+ = \sum_j T_{ij} S_{ja}^+ , \tag{A37}$$

where now $\underline{T}$ is to be evaluated at $\omega = 0$. Equation (A37) is of the form

$$[(\hbar\omega)^2 \underline{\alpha} + \hbar\omega \underline{\rho}]|\varphi\rangle = \underline{T}|\varphi\rangle , \tag{A38}$$

where

$$\alpha_{ij} = (2S)^{-1} \delta_{ij} \sum_k \frac{J_{ik}}{z_k^2 J^2} , \tag{A39a}$$

$$\rho_{ij} = \delta_{ij}\left(p_i - \sum_k \frac{J_{ik}}{J z_k}\right) . \tag{A39b}$$

We now proceed as for the ferrimagnet. We set

$$\underline{T} = \sum_n |\psi_n\rangle \lambda_n \langle\psi_n| . \tag{A40}$$

Using this expression, we rewrite (A38) as

$$\langle\psi_q|(\hbar\omega_q)^2 \underline{\alpha} + (\hbar\omega_q)\underline{\rho}|\varphi_q\rangle = \lambda_q \langle\psi_q|\varphi_q\rangle , \tag{A41}$$

in analogy with (A24). Following Brenig *et al.*, we write

$$|\psi_q\rangle = \exp(i\vec{q}\cdot\vec{r}_i)(1 + \vec{A}_i \cdot \vec{q}) p_i , \tag{A42a}$$

$$|\varphi_q\rangle = \exp(i\vec{q}\cdot\vec{r}_i)(1 + \vec{B}_i \cdot \vec{q} + C_i \hbar\omega_q) p_i , \tag{A42b}$$

$$\lambda_q/\hbar = D^* a^2 q^2 , \tag{A42c}$$

where D^* is the dispersion constant for the random network described by $\underline{T}$. The form (A42a) was previously given by Brenig *et al.*, and (A42b) follows in a similar way, except that an additional term of order $\omega_q \propto q$ is permitted in the antiferromagnet. Substituting these expressions into (A41) we obtain

$$D^* a^2 q^2 = (\hbar\omega_q)^2 \sum_{ij} \frac{J_{ij}}{(J z_j)^2 (2N_a S)} + \frac{\hbar\omega_q}{N_a} \sum_i (1 + \vec{A}_i^* \cdot \vec{q})\left(p_i - \sum_j \frac{J_{ij}}{J z_j}\right) \times (1 + \vec{B}_i \cdot \vec{q} + C_i \hbar\omega_q) , \tag{A43}$$

where

$$N_a = \sum_{i \in a} p_i . \tag{A44a}$$

Similarly, we define

$$N_b = \sum_{i \in b} p_i , \tag{A44b}$$

$$N = \sum_{i \in a} 1 = \sum_{j \in b} 1 . \tag{A44c}$$

We need to determine relations for $\vec{A}_i$, $\vec{B}_i$, and

C_i. To order q, $\underline{T}|\psi_n\rangle = \lambda_n|\psi_n\rangle$ yields

$$\sum_j T_{ij} \exp(i\vec{q}\cdot\vec{r}_j)(1+\vec{A}_j\cdot\vec{q}) = 0 \tag{A45a}$$

or

$$\sum_j T_{ij}[i\vec{q}\cdot(\vec{r}_j - \vec{r}_i) + \vec{A}_j\cdot\vec{q}] = 0\,. \tag{A45b}$$

To determine $\vec{B}_i$ and C_i we study (A38) to order q:

$$\hbar\omega_q\left(p_i - \sum_k \frac{J_{ik}}{Jz_k}\right) = \sum_j T_{ij}[i\vec{q}\cdot(\vec{r}_j - \vec{r}_i) + \vec{B}_j\cdot\vec{q} + \hbar\omega_q C_j]\,. \tag{A46}$$

We find that

$$\vec{B}_j = \vec{A}_j = -\vec{A}_j^*\,, \tag{A47}$$

since $\vec{A}_j$ is pure imaginary. For the antiferromagnetic case, ω_q is of order q, and we may therefore determine C_j from (A46):

$$C_j = \sum_l (\underline{T}^{-1})_{jl}\left(p_l - \sum_k \frac{J_{lk}}{z_k J}\right)\,. \tag{A48}$$

Since $\underline{T}$ has a zero eigenvalue associated with the uniform mode, its inverse, strictly speaking, does not exist. However, for the antiferromagnetic case, in which $N_a = N_b$, one can verify that $\underline{T}^{-1}$ in (A48) is applied to a vector which is orthogonal to the uniform mode, in view of the identity,

$$\sum_{j\in a}\left(p_j - \sum_k \frac{J_{jk}}{Jz_k}\right) = N_a - N_b\,. \tag{A49}$$

Using (A47)–(A49) we write (A43) as

$$(\hbar\omega_q)^2(M_a/N_a)\left[(2SJ)^{-1}\sum_{ij,i\in a}\frac{J_{ij}}{Jz_j^2} + \sum_{ij\in a}\left(p_i - \sum_k \frac{J_{ik}}{Jz_k}\right)(\underline{T}^{-1})_{ij}\left(p_j - \sum_k \frac{J_{jk}}{Jz_k}\right)\right] + (\hbar\omega_q)(M_a - M_b) - \hbar D^* M_a a^2 q^2 = 0\,, \tag{A50}$$

where M_a (M_b) is the magnetization of the a (b) sublattice: $M_a = N_a g\mu_B S/\Omega$ ($M_b = N_b g\mu_B S/\Omega$), and Ω is the volume of the system.

Note that by (A13b) we have $D^* M_a = 2\gamma A^*$, where A^* is the stiffness associated with $\underline{T}$. A^* is the same for ferromagnetic or antiferromagnetic nearest-neighbor interactions, and is proportional to the conductivity, A, of a network covering the two sublattices with $\sigma_{ij} = J_{ij}S_i^z S_j^z$. If we set $M_a - M_b = M$, then, for $M \neq 0$, (A50) becomes

$$\omega_q = (2\gamma A/M)q^2\,, \tag{A51}$$

in agreement with the hydrodynamic result for a ferromagnet.

We now show that for $M_a = M_b$, (A50) reproduces the results of the hydrodynamic treatment of an antiferromagnet. This will be true if the coefficient of $(\hbar\omega)^2$ in (A44) is $\chi_\perp/\hbar\gamma = \chi_\perp/g\mu_B$. We have defined

$$\chi_\perp = \frac{g\mu_B S}{h_0\Omega}\left(\sum_{i\in a} p_i\theta_i + \sum_{i\in b} p_j\theta_j\right), \tag{A52}$$

where θ is the solution to

$$\sum_j 2J_{ij}S(\theta_i + \theta_j) = g\mu_B h_0 \quad (p_i = 1)\,. \tag{A53}$$

Eliminating the b sites in (A53) we find that we can write $\chi_\perp$ in the form

$$\chi_\perp/g\mu_B = (S/h_0\Omega)\left[\frac{g\mu_B h_0}{2S}\sum_{j\in b}\frac{p_j}{Jz_j} + \sum_{i\in a}\left(p_i - \sum_j \frac{J_{ij}p_j}{Jz_j}\right)\theta_i\right], \tag{A54}$$

where θ_i satisfies

$$\sum_j T_{ij}\theta_j = g\mu_B h_0\left(p_i - \sum_j \frac{J_{ij}}{Jz_j}\right) \quad (i\in a)\,. \tag{A55}$$

Solving the equation for θ and inserting the result into (A54), we find an expression for $\chi_\perp/g\mu_B$ which agrees with the coefficient of $(\hbar\omega)^2$ in (A50). Thus (A50) reduces to

$$(\chi_\perp/g\mu_B)(\hbar\omega_q)^2 + (M_a - M_b)\hbar\omega_q - 2\hbar\gamma A q^2 = 0\,, \tag{A56}$$

in agreement with (20) and with hydrodynamics when $M_a = M_b$. The natural generalization to the case when $|(M_a - M_b)/M_a|$ is small but nonzero is to use $\chi_\perp$ as defined in Sec. IV in (A56). We have not been able to estimate the error introduced by this approximation.

APPENDIX B: EXACT SUSCEPTIBILITY FOR THE LINEAR CHAIN WITH CONNECTED ENDS

The susceptibility of a chain with connected ends ($J_N \neq 0$) can be obtained from χ^0 (65) by including J_N as a localized perturbation.[29] In this way one finds that

$$\begin{aligned}\chi(i,j) = \chi^0(i,j) &- [\xi_1\chi^0(i,1)/S_1 - \xi_N\chi^0(i,N)/S_N] \\ &\times [\xi_1\chi^0(1,j)/S_1 - \xi_N\chi^0(N,j)/S_N] \\ &\times [\sigma_N^{-1} + \chi^0(1,1)/S_1^2 + \chi^0(N,N)S_N^{-2} \\ &- 2\xi_1\xi_N\chi^0(1,N)/(S_1S_N)]^{-1}\,,\end{aligned} \tag{B1}$$

where we have assumed $\sigma_N \equiv 2J_N S_1 S_N \xi_1\xi_N > 0$. Explicitly, (B1) yields

$$\chi(1,n)=\frac{\xi_1\xi_N S_1 S_n}{R(NS_{\mathrm{av}}^2)^2}\left((NS_{\mathrm{av}}^2)\sum_{j=1}^{n-1}\sum_{k=n}^{N}\frac{U_k-U_j}{\sigma_j\sigma_k}+\sum_{j,k=1}^{N}\frac{(U_j-U_k)^2}{2\sigma_j\sigma_k}\right), \tag{B2}$$

where R is the resistance: $R=\sum_{j=1}^{N}\sigma_j^{-1}$ and S_{av}^2 and U are defined in (66). We define $\sum_{j=1}^{n-1}$ to be zero for $n=1$. Finally, to obtain $\chi(i,j)$ from $\chi(1,j-i+1)$ we suitably shift the site labels.

APPENDIX C: PROOF OF THE DIVERGENCE OF $\chi_\perp$ IN TWO DIMENSIONS

In this Appendix we refine the argument which led to the bound given in (134). We consider specifically the case $d=2$.

Let us apply (133) to an area $A_0=L^2$, assuming each spin S_i is governed by a Gaussian distribution of width σ_0. To make contact with the case of discrete occupancy variables one should interpret the S_i so distributed as representing an elementary volume unit consisting of sufficiently many sites that a continuous Gaussian distribution is appropriate. In that case $\sigma_0^2\sim x(1-x)$, but as we shall see, the size of σ_0 is irrelevant.

We use the result (133) to write

$$m_\perp\sim L^{-2}\int\left(\sum_{i\in A_0}S_i^2\right)\prod_{i\in A_0}[\varphi(S_i,0,\sigma_0^2)dS_i], \tag{C1}$$

where φ is a normalized Gaussian distribution:

$$\varphi(x,y,\sigma^2)=(2\pi\sigma^2)^{-1/2}\exp[-(x-y)^2/2\sigma^2]. \tag{C2}$$

Since independent Gaussians can be combined by adding their widths, one can express $m_\perp$ in terms of a distribution over the total spin S_0 in A_0 as

$$m_\perp\sim L^{-2}\int S_0^2\,\varphi(S_0,0,L^2\sigma_0^2)\,dS_0, \tag{C3}$$

which gives $m_\perp\sim\sigma_0^2$, in agreement with our earlier estimate.

Of course, one SDW for all of the A_0 is not a very good approximation to the state of lowest energy, especially when S_0 is small. Thus, when $|S_0|/L<\alpha_0\sigma_0$ for some α_0 to be determined, it is better to divide A_0 into n equal subvolumes and allow the unbalanced spin in each subvolume to form its own independent SDW. Thus we have

$$m_\perp\sim\frac{2}{L^2}\int_{L\alpha_0\sigma_0}^{\infty}S_0^2\,\varphi(S_0,0,L^2\sigma_0^2)dS_0+\frac{2}{L^2}\int_0^{L\alpha_0\sigma_0}\varphi(S_0,0,L^2\sigma_0^2)dS_0\sum_{i=1}^{n}S_i^2\,p(S_i,S_0)\prod_{i=1}^{n}dS_i, \tag{C4}$$

where $p(S_i,S_0)$ is the probability that the spin in the ith subvolume is S_i, subject to the constraint that $\sum_{i=1}^{n}S_i=S_0$. Since each S_i is governed by a Gaussian distribution, this constraint is easy to handle. One uses the relation

$$\int\prod_{i=1}^{n}\varphi(x_i,0,\sigma_0^2)\,\delta\left(X-\sum_{i=1}^{n}x_i\right)dx_2\,dx_3\cdots dx_n=\varphi(x_1,n^{-1}X,\sigma_0^2(n-1)/n). \tag{C5}$$

Thus,

$$p(S_i,S_0)=\varphi(S_i,n^{-1}S_0,L^2\sigma_0^2(n-1)/n^2). \tag{C6}$$

Introducing dimensionless variables we write (C4) as

$$m_\perp=\sigma_0^2+2\int_0^{\alpha_0\sigma_0}\varphi(x_0,0,\sigma_0^2)\left(-x_0^2+n\int\varphi(x_1,n^{-1}x_0,\sigma_0^2(n-1)/n^2)x_1^2dx_1\right)dx_0 \tag{C7a}$$

$$=\sigma_0^2\left(1+2[(n-1)/n]\int_0^{\alpha_0}\varphi(x_0,0,1)(1-x_0^2)\right)dx_0. \tag{C7b}$$

The optimum value of α_0 is clearly 1. The increase in $m_\perp$ from the second term in (C7b) is due to our better treatment of fluctuations of the unbalanced spin.

We now generalize the above construction having one stage of subdivision into one having r stages of subdivision. At the mth stage we establish SDW's only in those volume elements where the spin per site is larger than $\alpha_m\sigma_0$. If it is less than this value, we subdivide the volume element and repeat the criterion with each of the subvolumes so obtained. The state we are thereby describing is a mesh of differently sized SDW's tailored to take optimal advantage of the spin fluctuations. We find that

$$\frac{m_\perp}{\sigma_0^2}=1+\epsilon\int_{-\alpha_r}^{\alpha_r}\varphi_1(1-x_1^2)dx_1+\epsilon^2\int_{-\alpha_r}^{\alpha_r}dx_1\int_{-\alpha_{r-1}}^{\alpha_{r-1}}dx_2\,\varphi_1\varphi_2(1-x_2^2)+\cdots+\epsilon^r\int_{-\alpha_r}^{\alpha_r}dx_1\cdots\int_{-\alpha_1}^{\alpha_1}dx_r\prod_{i=1}^{r}\varphi_i(1-x_r^2), \tag{C8}$$

where $\epsilon=(n-1)/n$ and $\varphi_i=\varphi(x_i,0,1)$.

We will now show that if the α's are optimally chosen, this series diverges in the limit $\epsilon\to1, r\to\infty$. Since the size of A_0 must be at least of order $n^r=(1-\epsilon)^{-r}$, we see this limit corresponds to the infinite size limit of A_0.

We first determine the optimal values of the α's in (C8). Clearly $\alpha_1 = 1$. To optimize α_2, we combine the last two terms in the series of (C8), since these are the only ones involving α_2, Their sum is

$$\epsilon^{r-1}\int_{-\alpha_r}^{\alpha_r} dx_1 \cdots \int_{-\alpha_3}^{\alpha_3} dx_{r-2} \prod_{i=1}^{r-2} \varphi_i \int_{-\alpha_2}^{\alpha_2} dx_{r-1}\, \varphi_{r-1}[1 - x_{r-1}^2 + \epsilon I(\alpha_1)]\,, \tag{C9}$$

where

$$I(z) = \int_{-z}^{z} (z^2 - x^2)\varphi(x, 0, 1)dx\,. \tag{C10}$$

Evidently, optimization yields

$$\alpha_2^2 = 1 + \epsilon I(\alpha_1)\,. \tag{C11}$$

Proceeding in like fashion we see that

$$\alpha_{m+1}^2 = 1 + \epsilon I(\alpha_m)\,. \tag{C12}$$

Next we show that

$$1 = \alpha_1 < \alpha_2 < \cdots < \alpha_r\,. \tag{C13}$$

The proof is by induction. Clearly, according to (C11) $\alpha_1 < \alpha_2$. Next assume $\alpha_{m+1} > \alpha_m$. Then

$$\alpha_{m+2}^2 - \alpha_{m+1}^2 = \epsilon[I(\alpha_{m+1}) - I(\alpha_m)]\,, \tag{C14a}$$

$$\alpha_{m+2} - \alpha_{m+1} > 0\,, \tag{C14b}$$

since $I(z)$ is an increasing function of z. Therefore α_m increases with m and reaches a finite limit $\alpha_m \to \alpha$ only if

$$\alpha^2 = 1 + \epsilon I(\alpha) \tag{C15}$$

has a solution for finite α. We write this as

$$\alpha^2 - 1 = \epsilon(\alpha^2 - 1) + 2\epsilon \int_{\alpha}^{\infty} (\alpha^2 - x^2)\varphi(x, 0, 1)dx \tag{C16}$$

or

$$\alpha^2 - 1 = [2\epsilon/(1 - \epsilon)] \int_{\alpha}^{\infty} (\alpha^2 - x^2)\varphi(x, 0, 1)dx\,. \tag{C17}$$

The left-hand side of this equation increases monotonically from 0 to ∞ as α goes from 1 to ∞, and the right-hand side is a decreasing function of α for $\alpha > 1$. Therefore (C15) yields a unique solution for α. As $\epsilon \to 1, \alpha \to \infty$.

For large r the series in (C8) approximates a series of r terms with all α_i's equal to α. Thus for $\epsilon < 1$

$$m_\perp/\sigma_0^2 \sim \epsilon I(\alpha)\left(1 - 2\epsilon \int_0^{\alpha} \varphi(x, 0, 1)dx\right)^{-1}, \tag{C18}$$

which diverges as $\epsilon \to 1$ and $\alpha \to \infty$. More detailed analysis shows that this divergence is linear in r, and therefore equivalent to a divergence of the form $\ln N$, where N is the total number of sites.

APPENDIX D: INCREASE OF $\chi_\perp$ WITH DILUTION

The numerical studies of Sec. VII suggest that $\chi_\perp(p)$ for the infinite cluster increases monotonically as p decreases from unity, and diverges (or, for anisotropic systems, attains a maximum) at p_c. In this appendix we shall discuss the extent to which this behavior is a general consequence of dilution.

Intuitively, it is clear that $\chi_\perp$ should increase as the spins become less tightly connected. However, one can construct unusual situations in which the removal of selected spins will decrease $\chi_\perp$ for a particular sample. Thus, $\chi_\perp(p)$ can be a monotonic function of p only after appropriate averaging, or in the limit of an infinite sample. A weaker form of monotonic behavior can be proved for all samples. Since removing magnetic ions introduces the complication of a change in the number of degrees of freedom of the system, we consider instead a simpler process of dilution, namely one in which individual bonds are removed, i.e., individual J_{ij}'s are reduced to zero, without changing the number of spins in the cluster. We will now prove that this type of dilution always increases $\chi_\perp$.

Consider an arbitrary initial configuration, A, and write $\chi_\perp$ as

$$\chi_\perp^A = \kappa\langle 0|\underline{N}_A^{-1}|0\rangle\,. \tag{D1}$$

Here we use the notation of (73ff), κ is a constant, and the state $|0\rangle$ is defined by $\langle i|0\rangle = \sigma_i \equiv \langle S_i^z\rangle / |\langle S_i^z\rangle|$ on every site i. The existence of a finite $\chi_\perp^A$ implies that the configuration A does not contain any cluster consisting of an odd number of spins. If a bond is added to A, the susceptibility of the new configuration B is given by

$$\chi_\perp^B = \kappa\langle 0|\underline{N}_B^{-1}|0\rangle\,, \tag{D2}$$

and we wish to show that $\chi_\perp^A - \chi_\perp^B > 0$. If the added bond joins sites i and j, we have

$$\underline{N}_B = \underline{N}_A + \underline{V}\,, \tag{D3}$$

where

$$V_{kl} = 2JS(\delta_{ki} - \delta_{kj})(\delta_{li} - \delta_{lj})\,. \tag{D4}$$

Also we may write

$$\underline{N}_B^{-1} = \underline{N}_A^{-1} - \underline{N}_A^{-1}\,\underline{t}\,\underline{N}_A^{-1}\,, \tag{D5}$$

where

$$\underline{t} = \underline{V}(1 + \underline{N}_A^{-1}\,\underline{V})^{-1} \tag{D6}$$

is the single-bond t matrix. Inserting (D4) into (D6) we find that

$$t_{kl} = t_0(\delta_{ki} - \delta_{kj})(\delta_{li} - \delta_{lj}) , \tag{D7}$$

where

$$t_0 = 2JS(1 + 2JS\langle\varphi|\underline{N}_A^{-1}|\varphi\rangle)^{-1} , \tag{D8}$$

and $\varphi_k = \delta_{ki} - \delta_{kj}$. Thus,

$$\chi_\perp^A - \chi_\perp^B = 2JS\kappa t_0\langle 0|\underline{N}_A^{-1}|\varphi\rangle\langle\varphi|\underline{N}_A^{-1}|0\rangle \tag{D9a}$$

$$= 2JS\kappa t_0|\langle 0|\underline{N}_A^{-1}|\varphi\rangle|^2 . \tag{D9b}$$

To show that $\chi_\perp^A - \chi_\perp^B > 0$ we need only verify that $t_0 > 0$, which, according to (D8), will be true if $\langle\varphi|\underline{N}_A^{-1}|\varphi\rangle > 0$. We write

$$(\underline{N}_A^{-1})_{ij} = \sum_n{}' [|\psi_n(i)\rangle\langle\psi_n(j)|]/\lambda_n , \tag{D10}$$

where ψ_n λ_n are the eigenvectors and eigenvalues, respectively, of $\underline{N}_A$, and the prime indicates that $\lambda_n = 0$ is excluded from the summation. Thus,

$$\langle\varphi|\underline{N}_A^{-1}|\varphi\rangle = \sum_n{}' [|\psi_n(i) - \psi_n(j)|^2]/\lambda_n$$

$$> 0 \text{ Q.E.D.} \tag{D11}$$

---

*Supported in part by the Office of Naval Research under Grant No. N000 14-67-A-0216-0032, and by the National Science Foundation, MRL program, under Grant No. DMR72-03025.

[1]D. J. Breed, thesis (University of Amsterdam, 1969) (unpublished).

[2]D. J. Breed, K. Gilijamse, J. W. E. Sterkenberg, and A. R. Miedema, Physica (Utr.) 68, 303 (1973).

[3]D. J. Breed, K. Gilijamse, J. W. E. Sterkenberg, and A. R. Miedema, J. Appl. Phys. 41, 1267 (1970).

[4]S. Geller, H. J. Williams, G. P. Espinosa, and R. C. Sherwood, Bell Syst. Tech. J. 43, 565 (1964).

[5]E. C. Svensson, W. J. L. Buyers, T. M. Holden, R. A. Cowley, and R. W. H. Stevenson, AIP Conf. Proc. 5, 1315 (1972).

[6]R. J. Birgeneau, L. R. Walker, H. J. Guggenheim, J. Als-Nielsen, and G. Shirane, J. Phys. C 8, L328 (1975).

[7]J. Als-Nielsen, R. J. Birgeneau, H. J. Guggenheim, and G. Shirane, Phys. Rev. B 12, 4963 (1975).

[8]For example, see J. J. Rhyne, D. L. Price, and H. A. Mook, AIP Conf. Proc. 24, 121 (1975).

[9]S. Kirkpatrick and A. B. Harris, AIP Conf. Proc. 24, 99 (1975).

[10]S. Kirkpatrick, AIP Conf. Proc. 29, 141 (1976).

[11]S. Kirkpatrick, Solid State Commun. 12, 1279 (1973).

[12]D. Adler, L. P. Flora, and S. D. Senturia, Solid State Commun. 12, 9 (1973).

[13]B. I. Halperin and P. C. Hohenberg, Phys. Rev. 188, 898 (1969).

[14]For a review of percolation theory see V. K. S. Shante and S. Kirkpatrick, Adv. Phys. 20, 325 (1971); or J. W. Essam, in *Phase Transitions and Critical Phenomena*, edited by C. Domb and M. S. Green (Academic, New York, 1972), Vol. 2, p. 197.

[15]S. Chikazumi, *Physics of Magnetism* (Wiley, New York, 1966), p. 189.

[16]R. Wangsness, Phys. Rev. 91, 1085 (1953); 93, 68 (1954).

[17]S. Kirkpatrick and A. B. Harris, Phys. Rev. B 12, 4980 (1975).

[18]J. H. Van Vleck, Phys. Rev. 123, 58 (1961).

[19]The following example may clarify our choice of units: For a pure system on a body-centered-cubic lattice, where $J_{ij} = J$ when i and j are nearest neighbors, and is zero otherwise, and $\Delta_i = \Delta$, $K = \Delta S/2a^3$, $g\mu_B H_E = 16JS$, $A = 2JS^2/a$, $M = g\mu_B S/a^3$, where S is the spin and a is the lattice constant.

[20]J. Kaplan and C. Kittel, J. Chem. Phys. 21, 760 (1953).

[21]W. Brenig, P. Wölfle, and G. Dohler, Z. Phys. 246, 1 (1971).

[22]S. Kirkpatrick, Rev. Mod. Phys. 45, 574 (1973).

[23]In real systems there are always weak longer-range interactions which connect otherwise isolated clusters. For a given value of ω, clusters may be considered isolated if they are isolated when all interactions less than $\hbar\omega$ in energy are neglected. Our treatment is thus valid for frequencies such that only nearest-neighbor interactions are important.

[24]J. C. Scott, A. F. Garito, A. J. Heeger, P. Nannelli, and H. D. Gillman, Phys. Rev. B 12, 356 (1975).

[25]T. S. Wei, J. C. Scott, A. F. Garito, A. J. Heeger, H. D. Gillman, and P. Nanelli, Phys. Rev. B 12, 5297 (1975).

[26]This is the usual (see Ref. 27) definition of a Green's function for a system of linear equations having a homogeneous solution. We may also express $\underline{G}$ in operator form as $\sum_n{}'|\varphi_n\rangle\underline{D}^{-1}\langle\varphi_n|$, where $|\varphi_n\rangle$ is the nth eigenvector and the prime indicates omission of the terms with vanishing eigenvalues.

[27]P. Dennery and A. Krzywicki, *Mathematics for Physicists* (Harper and Row, New York, 1967), p. 284.

[28]Y. Izyumov, Proc. Phys. Soc. Lond. 87, 505 (1966).

[29]G. F. Koster and J. C. Slater, Phys. Rev. 95, 1167 (1954).

[30]A. B. Harris, P. L. Leath, B. G. Nickel, and R. J. Elliott, J. Phys. C 7, 1693 (1974).

[31]T. Tonegawa and J. Kanamori, Phys. Lett. 21, 130 (1966); T. Tonegawa, Progr. Theor. Phys. 40, 1195 (1968).

[32]S. W. Lovesey, J. Phys. C 1, 102 (1968).

[33]B. Dreyfus, J. Appl. Phys. 34, 1089 (1963).

[34]There are some misprints in I. In (29) and (B8c) the plus signs should be minus signs. (The results obtained in I were calculated with the correct signs.) To clarify the notation of Appendix B of I: The t matrix $t_\alpha(\omega)$ is that for a defect on the up ($\sigma_i = +1$) sublattice, and for $\alpha \neq s$, $V_\alpha = 2(J_A S_A - J_B S_B)$, where A refers to the host and B to the defect. For $\alpha = s$, the t matrix is given explicitly by (B4) of I.

[35]F. M. Johnson and A. H. Nethercot, Jr., Phys. Rev. 114, 705 (1959).

[36]L. J. deJongh and A. R. Miedema, Adv. Phys. 23, 1 (1974).
[37]G. S. Rushbrooke and D. J. Morgan, Mol. Phys. 4, 1 (1961).
[38]G. S. Rushbrooke and P. J. Wood, Mol. Phys. 1, 257 (1958).
[39]G. S. Rushbrooke, in *Critical Phenomena in Alloys, Magnets and Superconductors*, edited by R. E. Mills, E. Ascher, and R. I. Jaffee (McGraw-Hill, New York, 1971), p. 155.
[40]G. S. Rushbrooke, R. A. Muse, R. L. Stephenson, and K. Pirnie, J. Phys. C 5, 3371 (1972).
[41]B. P. Watson and P. L. Leath, Phys. Rev. B 9, 4893 (1974); 12, 498(E) (1975).
[42]S. Kirkpatrick, Phys. Rev. Lett. 27, 1722 (1971).
[43]H. W. de Wijn, R. E. Walstedt, L. R. Walker, and H. J. Guggenheim, J. Appl. Phys. 42, 1595 (1971).
[44]P. T. Woo, S. J. Roberts, and F. G. Gustavson, Society of Petroleum Engineers (AIME) Journal (1974).
[45]J. C. Slonczewski, A. P. Malozemoff, and E. A. Giess, Appl. Phys. Lett. 24, 396 (1974).
[46]P. W. Kasteleyn and C. M. Fortuin, J. Phys. Soc. Jpn. Suppl. 26, 11 (1969); C. M. Fortuin and P. W. Kasteleyn, Physica (Utr.) 57, 536 (1972); C. M. Fortuin, *ibid.* 58, 393 (1972); 59, 545 (1972).
[47]A. B. Harris, T. C. Lubensky, W. K. Holcomb, and C. Dasgupta, Phys. Rev. Lett. 35, 327 (1975); 35, 1397(E) (1975).
[48]D. Stauffer, Phys. Rev. Lett. 35, 394 (1975).
[49]S. Kirkpatrick, Phys. Rev. Lett. 36, 69 (1976).
[50]M. F. Sykes, M. Glen, and D. S. Gaunt, J. Phys. A 7, L105 (1974).
[51]M. E. Fisher and J. W. Essam, J. Math. Phys. 2, 609 (1961).
[52]M. E. Levinshtein, B. I. Shklovski, M. S. Shur, and A. L. Efros, Zh. Eksp. Teor. Fiz. 69, 386 (1975) [Sov. Phys.-JETP 42, 197 (1976)].
[53]G. Toulouse, Nuovo Cimento 23, 234 (1974).
[54]P. G. de Gennes, J. Phys. Lett. 37, L1 (1976). Rather similar physical pictures have independently been suggested by A. Skal and B. I. Shklovskii, Fiz. Tekn. Poluprovodn. 8, 1586 (1974) [Sov. Phys.-Semicond. 8, 1029 (1975)] and D. Stauffer, Z. Phys. B 22, 161 (1975).
[55]R. B. Stinchcombe, J. Phys. C 7, 179 (1974).
[56]For definitions of "nodes" and the effective length L see Ref. 54 and G. R. Dobson and M. Gordon, J. Chem. Phys. 43, 705 (1965).
[57]A similar argument has been given by Y. Imry and S.-K. Ma [Phys. Rev. Lett. 35, 1399 (1975)] for the behavior of a uniform system in a spatially random applied field.
[58]L. P. Kadanoff, Physics (N.Y.) 2, 263 (1966).
[59]R. Alben and M. F. Thorpe, J. Phys. C 8, L275 (1975).
[60]R. C. LeCraw, J. P. Remeika, and H. Matthews, J. Appl. Phys. 36, 901 (1965).
[61]B. Luthi, Phys. Rev. 148, 519 (1966).
[62]S. Geller, J. A. Cape, G. P. Espinosa, and D. H. Leslie, Phys. Rev. 148, 522 (1966).
[63]P. J. Wojtowicz, Phys. Lett. 11, 18 (1964).
[64]R. Gonano, E. Hunt, and H. Meyer, Phys. Rev. 156, 521 (1967).
[65]J. P. van der Ziel, J. F. Dillon, and J. P. Remeika, AIP Conf. Proc. 5, 254 (1972).
[66]P. J. Wojtowicz, J. Appl. Phys. 33, 1257S (1962).
[67]A. Rosencwaig, Can. J. Phys. 48, 2857 (1970); 48, 2868 (1970).
[68]S. Geller, J. Appl. Phys. 37, 1408 (1966); Phys. Rev. 181, 980 (1969).
[69]M. A. Gilleo and S. Geller, Phys. Rev. 110, 73 (1957).
[70]R. D. Henry and D. M. Heinz, AIP Conf. Proc. 18, 194 (1973).
[71]R. D. Enoch, M. E. Jones, and D. G. P. Waters, Appl. Phys. Lett. 26, 127 (1975).
[72]A. B. Harris and H. Meyer, Phys. Rev. 127, 101 (1962).
[73]B. Dreyfus, J. Phys. Chem. Solids 23, 287 (1962).
[74]M. Tinkham, Phys. Rev. 124, 311 (1961).
[75]Y. Ayant and G. Thomas, C. R. Acad. Sci. (Paris) 250, 2688 (1960).
[76]A. B. Harris, Phys. Rev. 132, 2398 (1963).
[77]A. J. Sievers and M. Tinkham, Phys. Rev. 124, 321 (1961); Phys. Rev. 129, 1995 (1963).
[78]R. Pauthenet, C. R. Acad. Sci. (Paris) 242, 1859 (1956); Ann. Phys. (Paris) 3, 424 (1958); J. Phys. Rad. 20, 38 (1959).
[79]R. B. Stinchocombe and B. P. Watson, J. Phys. C 9, 3221 (1976); J. P. Straley (unpublished); S. Kirkpatrick (unpublished).